Article

Cell Reports

Evolutionary Divergence of Enzymatic Mechanisms for Tubulin Detyrosination

Graphical Abstract

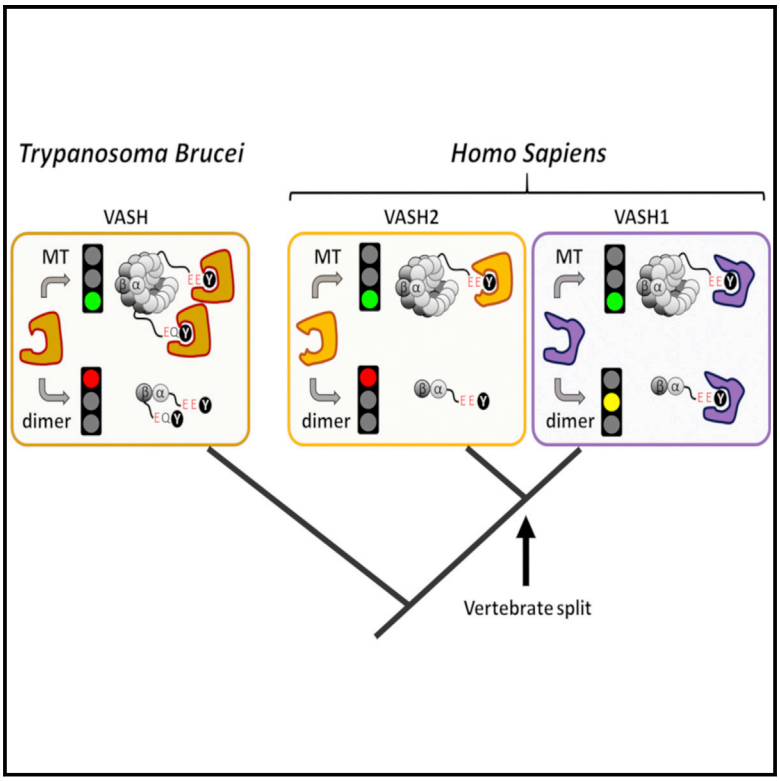

Authors

Siem van der Laan, Maude F. Lévêque, Guillaume Marcellin, ..., Yvon Sterkers, Patrick Bastien, Krzysztof Rogowski

Correspondence

siem.vanderlaan@igh.cnrs.fr (S.v.d.L.), maude.leveque@umontpellier.fr (M.F.L.), krzysztof.rogowski@igh.cnrs.fr (K.R.)

In Brief

van der Laan et al. describe the evolutionary diversification of the VASH-mediated mechanism of tubulin detyrosination . In addition, they show that this modification plays an important role in *Trypanosoma* parasites, where it regulates cell division and cell morphology.

Highlights

- In contrast to VASH1, VASH2 does not require SVBP for detyrosinating activity
- Diversification of tubulin detyrosination coincides with the appearance of vertebrates
- TbVASH detyrosinates both α- and β-tubulin tails of *Trypanosoma brucei*
- Parasites lacking TbVASH grow slowly and display severe morphological abnormalities

van der Laan et al., 2019, Cell Reports *29*, 4159–4171
December 17, 2019
https://doi.org/10.1016/j.celrep.2019.11.074

CellPress

Cell Reports
Article

Evolutionary Divergence of Enzymatic Mechanisms for Tubulin Detyrosination

Siem van der Laan,[1,7,*] Maude F. Lévêque,[2,7,*] Guillaume Marcellin,[1] Lubomir Vezenkov,[3] Yoann Lannay,[1] Geronimo Dubra,[1] Guillaume Bompard,[1] Sara Ovejero,[1] Serge Urbach,[4] Andrew Burgess,[5,6] Muriel Amblard,[3] Yvon Sterkers,[2] Patrick Bastien,[2] and Krzysztof Rogowski[1,8,*]

[1]Tubulin Code Team, Institute of Human Genetics (IGH), CNRS-Université Montpellier, 141 rue de la Cardonille, 34293 Montpellier Cedex 5, France

[2]Université Montpellier-CNRS, "MiVEGEC," Faculté de Medicine and Centre Hospitalier Universitaire, 39 avenue Charles Flahault, 34295 Montpellier Cedex 5, France

[3]Institut des Biomolécules Max Mousseron (IBMM), UMR 5247, CNRS-Université Montpellier-ENSCM, 34093 Montpellier Cedex 5, France

[4]Functional Proteomics Platform (FPP), IGF, Université Montpellier, CNRS, INSERM, Montpellier, France

[5]ANZAC Research Institute, Gate 3 Hospital Rd., Concord, Sydney, NSW 2139, Australia

[6]The University of Sydney Concord Clinical School, Faculty of Medicine and Health, Sydney, NSW, Australia

[7]These authors contributed equally

[8]Lead Contact

*Correspondence: siem.vanderlaan@igh.cnrs.fr (S.v.d.L.), maude.leveque@umontpellier.fr (M.F.L.), krzysztof.rogowski@igh.cnrs.fr (K.R.)

https://doi.org/10.1016/j.celrep.2019.11.074

SUMMARY

The two related members of the vasohibin family, VASH1 and VASH2, encode human tubulin detyrosinases. Here we demonstrate that, in contrast to VASH1, which requires binding of small vasohibin binding protein (SVBP), VASH2 has autonomous tubulin detyrosinating activity. Moreover, we demonstrate that SVBP acts as a *bona fide* activator of both enzymes. Phylogenetic analysis of the vasohibin family revealed that regulatory diversification of VASH-mediated tubulin detyrosination coincided with early vertebrate evolution. Thus, as a model organism for functional analysis, we used *Trypanosoma brucei* (Tb), an evolutionarily early-branched eukaryote that possesses a single VASH and encodes a terminal tyrosine on both α- and β-tubulin tails, both subject to removal. Remarkably, although detyrosination levels are high in the flagellum, TbVASH knockout parasites did not present any noticeable flagellar abnormalities. In contrast, we observed reduced proliferation associated with profound morphological and mitotic defects, underscoring the importance of tubulin detyrosination in cell division.

INTRODUCTION

Microtubules (MTs) are major cytoskeletal elements of eukaryotic cells and are involved in numerous cellular functions, including intracellular transport, cell motility, cell division, and cell morphogenesis. They are formed by polymerization of a heterodimer composed of two globular proteins, α- and β-tubulin. Each particular MT function requires recruitment of a specific set of MT-associated proteins (MAPs) and molecular motors, many of which have been shown to interact specifically with the C-terminal tails of tubulins that protrude from the MT surface (Ciferri et al., 2008; Mizuno et al., 2004; Roll-Mecak and Vale, 2008; Skiniotis et al., 2004). One of the mechanism by which MTs adapt their function to the changing biological needs of a cell is by regulating the type and extent of posttranslational modifications (PTMs) on the protruding C-terminal tails of α- and β-tubulin. Therefore, specific MAPs are recruited to execute the appropriate function (Verhey and Gaertig, 2007; Westermann and Weber, 2003). The first PTM to be discovered was detyrosination (Barra et al., 1974). It consists of proteolytic removal of the very C-terminal tyrosine residue from α-tubulin, resulting in generation of so-called Δ1-tubulin. This PTM is reversible, and addition of tyrosine is carried out by tubulin-tyrosine ligase (TTL). The cycle of tyrosination and detyrosination is evolutionary conserved from unicellular early-branched eukaryotes, such as *Trypanosoma*, to humans (Preston et al., 1979).

During mitosis, Δ1-tubulin is exclusively found in the peripheral regions of half spindles and appears to be absent from astral fibers (Akera et al., 2017; Gundersen and Bulinski, 1986a; Winkelhaus and Hauser, 1997). Recent studies have shown that spindle detyrosination is essential for correct chromosome congression (Barisic et al., 2015). Moreover, detyrosination has also been shown to play an important role in symmetry breakage during female meiosis, for advantageous segregation of selfish elements that can enhance their transmission, through a process known as meiotic drive (Akera et al., 2017; Barisic et al., 2015). Both observations suggest an essential role of this modification in maintenance of genomic stability. In addition, high levels of Δ1-tubulin have also been observed on stable MT assemblies such as axonemes, centrioles, and basal bodies, suggesting that detyrosination may also be of functional importance in the assembly and maintenance of these structures (Gundersen and Bulinski, 1986a). Furthermore, detyrosination has been found to be important during cellular differentiation events, including myogenesis (Chang et al., 2002; Gundersen et al.,

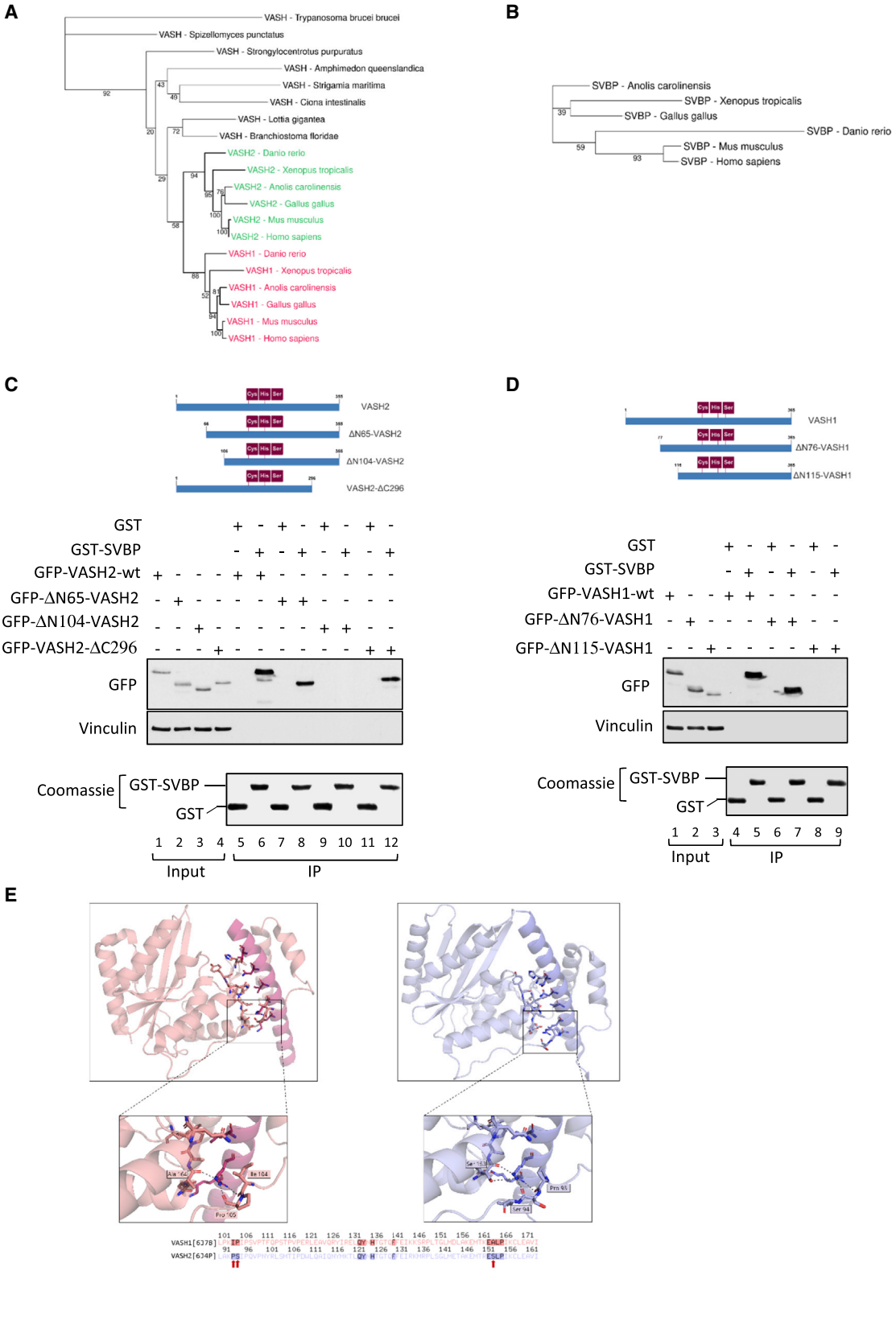

(legend on next page)

1989; Kerr et al., 2015) and neurogenesis (Aillaud et al., 2017; Cambray-Deakin and Burgoyne, 1987; Erck et al., 2005), where it accumulates mostly on stable MTs.

By using non-specific protease inhibitors, we found previously that tubulin detyrosinase is a cysteine protease. This type of protease is amenable to covalent inhibition by reactive chemical warheads, such as epoxide (Albeck and Kliper, 1997). Therefore, by fusing epoxide to different numbers of amino acids corresponding to the very C terminus of α-tubulin, we obtained compounds that inhibited detyrosinase activity in brain extracts. Using a biochemical approach consisting of covalent inhibitors compatible with click chemistry, we identified two members of the vasohibin family, VASH1 and VASH2, as tubulin detyrosinases (Aillaud et al., 2017). This was a major breakthrough in the field, opening up the possibility to perform direct functional studies and to finally get a better understanding of the evolutionary history of tubulin detyrosination.

Here we performed a phylogenetic analysis of the vasohibin protein family together with its chaperone, small vasohibin binding protein (SVBP). Our analysis revealed that regulatory diversification of VASH-mediated tubulin detyrosination coincided with early vertebrate evolution. In turn, we used *Trypanosoma brucei* (Tb), an evolutionarily early-branched eukaryote that possesses only a single VASH, as a model organism for functional analysis of tubulin detyrosination. We found that deletion of the VASH gene in these parasites results in severely defective morphogenesis and growth reduction. Although detyrosination in most species is specific to α-tubulin, trypanosomatid parasites are unique in that their β-tubulin also carries a tyrosine at the C-terminal end, which is also subject to removal (Schneider et al., 1997). We show that TbVASH removes the C-terminal tyrosine residue of both α- and β-tubulin, accommodating both tubulin tails in its enzymatic pocket. This specific trait provides the opportunity to design peptide-based inhibitors that preferentially target TbVASH. We propose that TbVASH may be an exploitable target for development of drugs against trypanosomatid-related diseases.

RESULTS

SVBP Is a *Bona Fide* Activator of VASH-Mediated Tubulin Detyrosination

To gain a better understanding of the evolutionary relationship between VASH enzymes and SVBP, we performed phylogenetic analysis of both families using sequences from diverse eukaryotic organisms. A protein phylogeny of the VASH family revealed three distinct clades: VASH1- and VASH2-related proteins from vertebrates and a clade grouping VASH sequences from invertebrates (Figure 1A). Of note, despite the documented presence of detyrosination in *Caenorhabditis elegans* and *Drosophila melanogaster* (O'Hagan et al., 2011; Warn et al., 1990), Basic Local Alignment Search Tool (Blastp) results did not retrieve any VASH homologs, suggesting the existence of alternative tubulin detyrosinating enzymes. By using publicly available sequences, we also constructed a phylogenetic tree of SVBP (Figure 1B). We observed that the sequence homology within the vertebrate lineage was very high, and blastp search for SVBP sequences outside of vertebrates did not identify homologous genes. In view of the rounds of whole-genome duplication that occurred in early vertebrate evolution (Meyer and Schartl, 1999), the appearance of VASH1 and VASH2 proteins as separate genes may have emerged as a consequence of this phenomenon.

Because both VASH1 and VASH2 are enzymatically active (Figure S1A), and both enzymes bind to SVBP (Suzuki et al., 2010), we expressed a number of previously described natural isoforms of VASH2 (Sato, 2013) in HEK293 cells and performed pull-down assays using either glutathione S-transferase (GST) or GST-SVBP to more precisely map the interaction domains. We observed that full-length VASH2, ΔN65-VASH2, and the C-terminally truncated VASH2-ΔC296 all associated with SVBP whereas ΔN104-VASH2 did not (Figure 1C). Furthermore, the association between SVBP and VASH was independent of its catalytic activity (Figure S1B). Because no evidence of similar VASH1 splice variants could be found in the Ensembl database (http://www.ensembl.org/index.html) http://www.ensembl.org//useast.ensembl.org/?redirectsrc=//www.ensembl.org%2F, we generated homologous truncations of VASH1 based on the naturally occurring VASH2 isoforms. Similarly, full-length VASH1 and ΔN76-VASH1 interacted with SVBP (Figure 1D) whereas ΔN76–115-VASH1 did not. Similarly, to VASH2 the association of SVBP was independent of the enzymatic activity (Figure S1C). Altogether, these data indicate that binding occurs through the corresponding region of VASH2 (N-terminal residues 66–104) and VASH1 (N-terminal 76–115), a domain we termed the SVBP-binding site (SVBP-BS). The very recent structural data obtained for VASH1 and VASH2 (Adamopoulos et al., 2019; Liao et al., 2019) allowed structural alignment of the SVBP-BS region (Figure 1E) and confirmed the presence of important residues within this region that are involved in interaction with SVBP. Remarkably, co-transfection of either VASH1 or VASH2 with SVBP resulted in a marked increase in total tubulin detyrosination compared with cells transfected with the enzymes alone (Figures 2A and 2B). Similar activation was observed for the intermediate N-terminal truncations of VASH2, which still contained the SVBP binding site (Figure 2A). In contrast, activation of both VASHs

Figure 1. The Appearance of hVASH1 and hVASH2 Coincides with Branching of the Vertebrate Lineage

(A) Phylogenetic tree of the VASH protein family, constructed with homologous sequences of a number of model organisms.

(B) Phylogenetic tree of the SVBP protein family, constructed with homologous sequences of a number of model organisms.

(C) SVBP binds to the N-terminal domain of VASH2, comprising amino acids 65–104 (naturally occurring variants). Shown are GST-SVBP pull-down assays of ectopically expressed VASH2 constructs in HEK293 cells. Samples were immunoblotted using the indicated antibodies.

(D) SVBP binds to the N-terminal domain, comprising amino acids 76–115 of VASH1 (constructs that reflect the natural variants of VASH2). Shown are GST-SVBP pull-down assays of ectopically expressed VASH1 constructs in HEK293 cells. Samples were immunoblotted using the indicated antibodies.

(E) Structural alignment of VASH1 (PDB: 6J7B; red) and VASH2 (PDB: 6J4P; blue) using PyMOL software. The insets show one of the interaction domains with SVBP and the key residues involved in interaction.

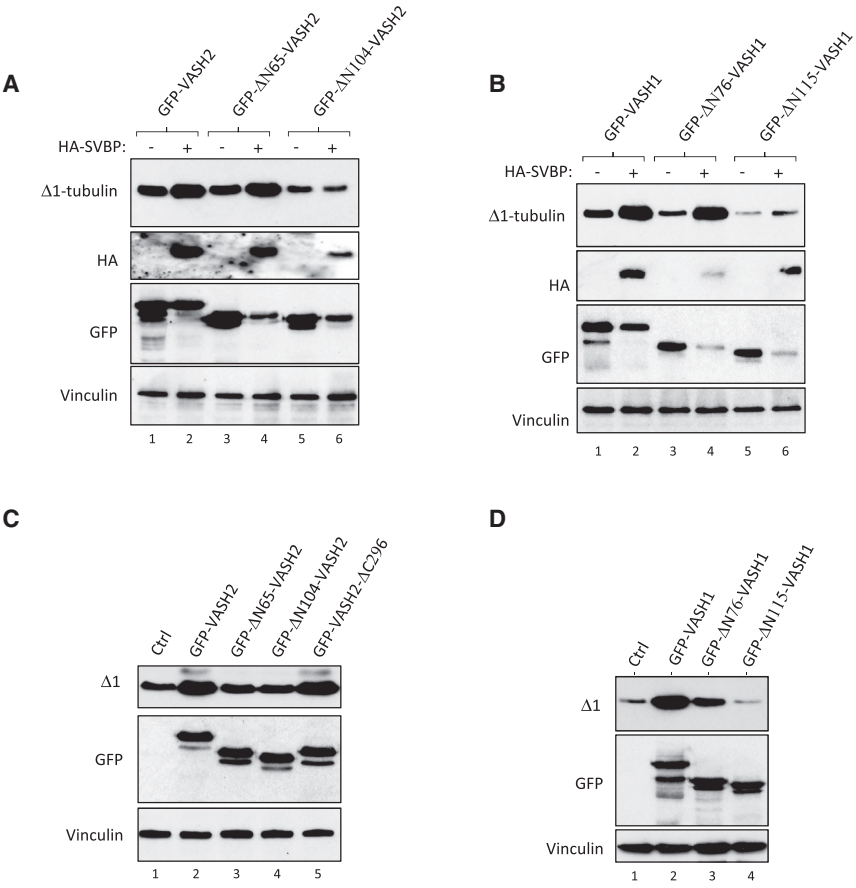

Figure 2. SVBP Acts as Activator of VASH-Mediated Tubulin Detyrosination *In Cellulo*

(A) Expression of SVBP activates VASH2-mediated tubulin detyrosination in human HEK293 cells. Twenty-four h after transfection with the indicated plasmids, cells were collected and analyzed by immunoblotting with the indicated antibodies.

(B) Expression of SVBP activates VASH1-mediated tubulin detyrosination in human HEK293 cells. Twenty-four h after transfection with the indicated plasmids, cells were collected and analyzed by immunoblotting with the indicated antibodies.

(C) Expression of VASH2 isoforms in human HEK293 cells. Shown is expression of full-length VASH2 and three additional occurring isoforms. Twenty-four h after transfection with the indicated plasmids, cells were collected and analyzed by immunoblotting with the indicated antibodies.

(D) Expression of VASH1 isoforms in human HEK293 cells. Shown is expression of full-length VASH1 and two N-terminally truncated isoforms. Twenty-four h after transfection with the indicated plasmids, cells were collected and analyzed by immunoblotting with the indicated antibodies.

was completely lost upon removal of the N-terminal part that contains the SVBP binding site (Figures 2C and 2D), demonstrating that this part of the sequence is required for binding and mediates activation of the detyrosinating activity (Figures S2A and S2B).

VASH2 Acts as an Autonomous Tubulin Detyrosinase

Historically, most *in vitro* MT-based assays involved the use of tubulin purified from pig brain. However, brain tubulin carries high levels of detyrosination, greatly complicating analysis of VASH activity. In search of a source of an unmodified substrate, we found that tubulin purified from *Spodoptera frugiperda*-derived Sf9 cells (Figure 3A) is fully tyrosinated; this modification could not be detected by mass spectrometry analysis (Figure 3B). Therefore, we generated an antibody against the detyrosinated C-terminal sequence of *Spodoptera frugiperda* α-tubulin (-EGEGAEE) and tested its specificity compared with the commonly used anti-murine Δ1-tubulin antibody. Our results clearly show that detyrosinated Sf9 tubulin is specifically recognized by our newly developed antibody but not by the commonly used murine counterpart (Figure 3C). Therefore, using purified bacterially produced recombinant human VASH1 and VASH2 proteins and MTs assembled from purified Sf9 tubulin, we performed *in vitro* detyrosination assays. Although VASH2 displayed strong detyrosinase activity, recombinant hVASH1, surprisingly, appeared to be inactive (Figure 3D). Because we previously found that SVBP has the ability to increase detyrosinase activity in human HEK293 cells (Figures 2A and 2B), we co-transformed bacteria to produce recombinant VASH1 or VASH2 in complex with SVBP. Strikingly, we observed high detyrosinating activity for the VASH1/SVBP complex, whereas VASH1 alone was inactive (Figure 3E). In contrast to VASH1, VASH2 displayed autonomous detyrosinase activity that was further increased by ectopic addition of recombinant SVBP, supporting the notion that SVBP acts as a *bona fide* activator (Figures S3A and S3B, compare lanes 2 and 3). To test whether the activatory role of SVBP is mediated by increasing the affinity of VASH1 for MTs, we performed turbidimetry and co-sedimentation assays. Both approaches showed no measurable change in the affinity of VASH1 for MTs regardless of the presence or absence of SVBP (Figures S3C and S3D). Next we compared the kinetics of both enzymes in complex with SVBP. Unexpectedly, the SVBP/VASH1 complex displayed substantial detyrosinating activity toward the free tubulin dimer (Figure 3F, top panel; Figure S3E), whereas SVBP/VASH2 appeared to specifically modify microtubule filaments despite having much higher overall detyrosinating activity (Figure 3F, bottom panel; Figure S3F). Taken together, our data demonstrate that SVBP acts as an essential partner for VASH1-mediated tubulin detyrosinase whereas it is dispensable for VASH2.

The *Trypanosoma brucei* VASH Homolog Catalyzes Tubulin Detyrosination

Because the presence of two VASH genes and expression of a naturally detyrosinated α4-tubulin isoform in vertebrates complicates phenotypic analysis in human cells, we used *Trypanosoma brucei* as a model organism. Strikingly, although detyrosination

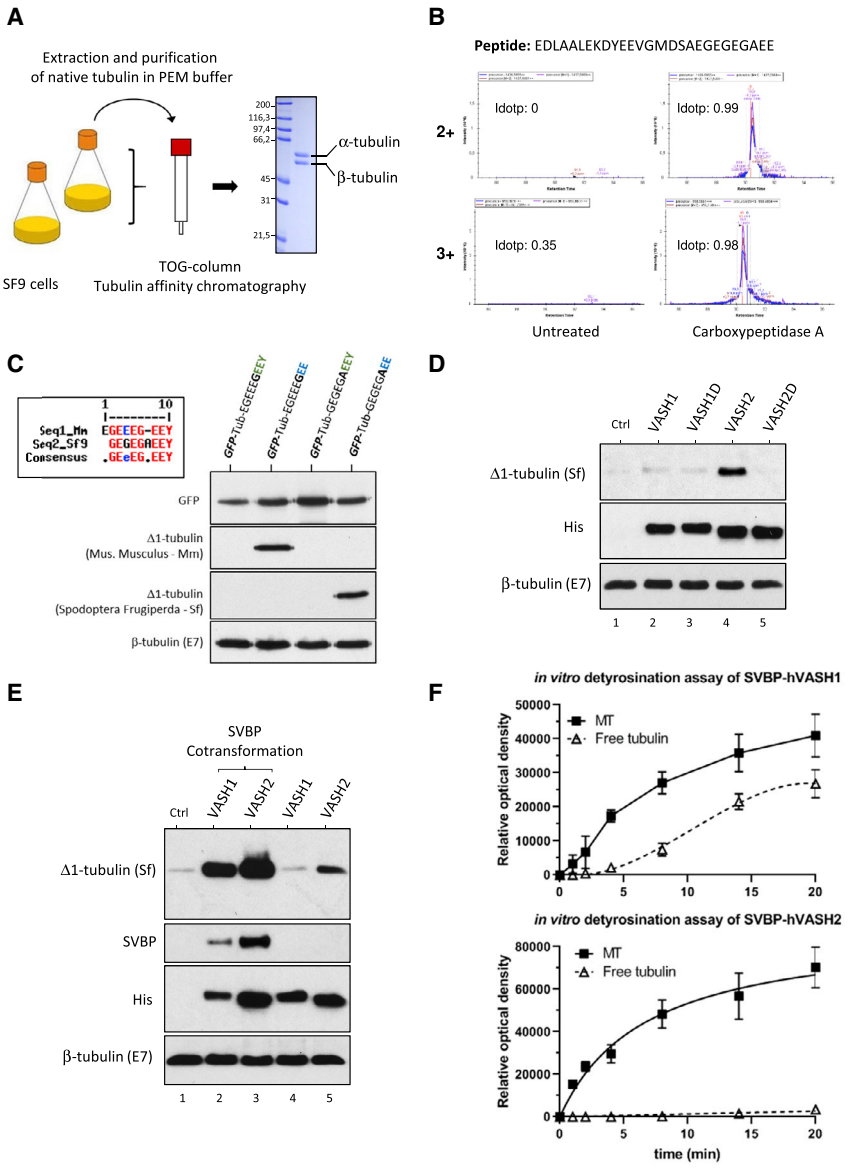

Figure 3. The Presence of SVBP Is Fundamental for VASH1-Mediated Tubulin Detyrosination

(A) Schematic representation of tubulin purification from the *Spodoptera frugiperda* Sf9 cell line.

(B) Mass spectrometry analysis of non-treated or carboxypeptidase A (CPA)-treated microtubules generated from purified tubulin of Sf9 cells. The signal was obtained for EDLAALEKDYEEVGMD SAEGEGEGAEE (2+ and 3+) left untreated (left) or CPA treated (right). Isotopic dot product scores show a good correlation for the treated sample (close to 1) and no correlation with the background signal in the untreated sample.

(C) Characterization of the *Spodoptera frugiperda*-specific Δ1-tubulin antibody. Shown is immunoblot analysis of HEK cells transfected with the indicated expression plasmids. Twenty-four h after transfection, samples were collected and analyzed by immunoblotting with the indicated antibodies.

(D) *In vitro* detyrosination assay using recombinant VASH1 and VASH2 proteins and their respective dead mutants (Cys-Ala). The assay was performed on MTs polymerized from Sf9-purified tubulin. Reactions were stopped after 30 min and analyzed by immunoblotting with the indicated antibodies.

(E) *In vitro* detyrosination assay of purified recombinant VASH1 and VASH2 produced in bacteria in the absence or presence of SVBP (co-transformation). Reactions were stopped after 30 min and analyzed by immunoblotting with the indicated antibodies.

(F) *In vitro* time course analysis of VASH1- and VASH2-mediated tubulin detyrosination in the presence of SVBP. Tubulin detyrosination activity was measured under suboptimal conditions. Samples were analyzed by immunoblotting, and relative optical density of three independent assays was measured (n = 3; error bars represent SEM).

See Figures S3E and S3F for representative immunoblots.

in most species is specific to α-tubulin, trypanosomatid parasites encode a β-tubulin, which also ends with a tyrosine and appears to be subject to removal (Schneider et al., 1997). PTMs of tubulin, and specifically α-tubulin detyrosination, are well-documented in Tb, which assembles a number of elaborated MT-based structures, such as sub-cortical arrays, flagella, or mitotic spindles (Gull, 1999). We aligned the amino acid sequences of human VASH1 and VASH2 with that of TbVASH and found that the catalytic triad containing the essential cysteine residue was present within its central domain (Figure 4A). Overall, TbVASH displayed a slightly higher similarity to hVASH2 than to hVASH1 (Figure S4A) and, intriguingly, contained a putative nuclear localization signal (NLS) that was also present in hVASH2 (Figure 4B). In light of the closed mitosis in *Trypanosoma*, the presence of an NLS motif in TbVASH suggests that spindle detyrosination might occur directly in the nucleus. Expression of wild-type but not the catalytically dead variant of TbVASH in human HEK293 cells resulted in a strong increase in α-tubulin detyrosination, as observed by immunoblot analysis of protein lysates (Figure 4C) and by immunofluorescence analysis (Figure S4B). Using the *in vitro* assay described above (Figure 3), we showed that recombinant TbVASH completely removed the C-terminal tyrosine from α-tubulin and, similar to hVASH2, displayed autonomous catalytic activity (Figure 4D). Moreover, we found that TbVASH specifically detyrosinates microtubules and showed no significant activity toward free tubulin dimers (Figures 4E and S4C). Next, although no ortholog of the SVBP gene could be found in the *T. brucei* genome, we sought to test whether TbVASH contains the putative SVBP-BS. Based on the structural alignment of the N-terminal amino acids of TbVASH to the corresponding domains of vertebrate proteins, we found that previously described key residues were also present in TbVASH (Figure 4F). Pull-down assays using either full-length TbVASH or Tb-ΔN38-VASH and GST-tagged SVBP surprisingly demonstrated that

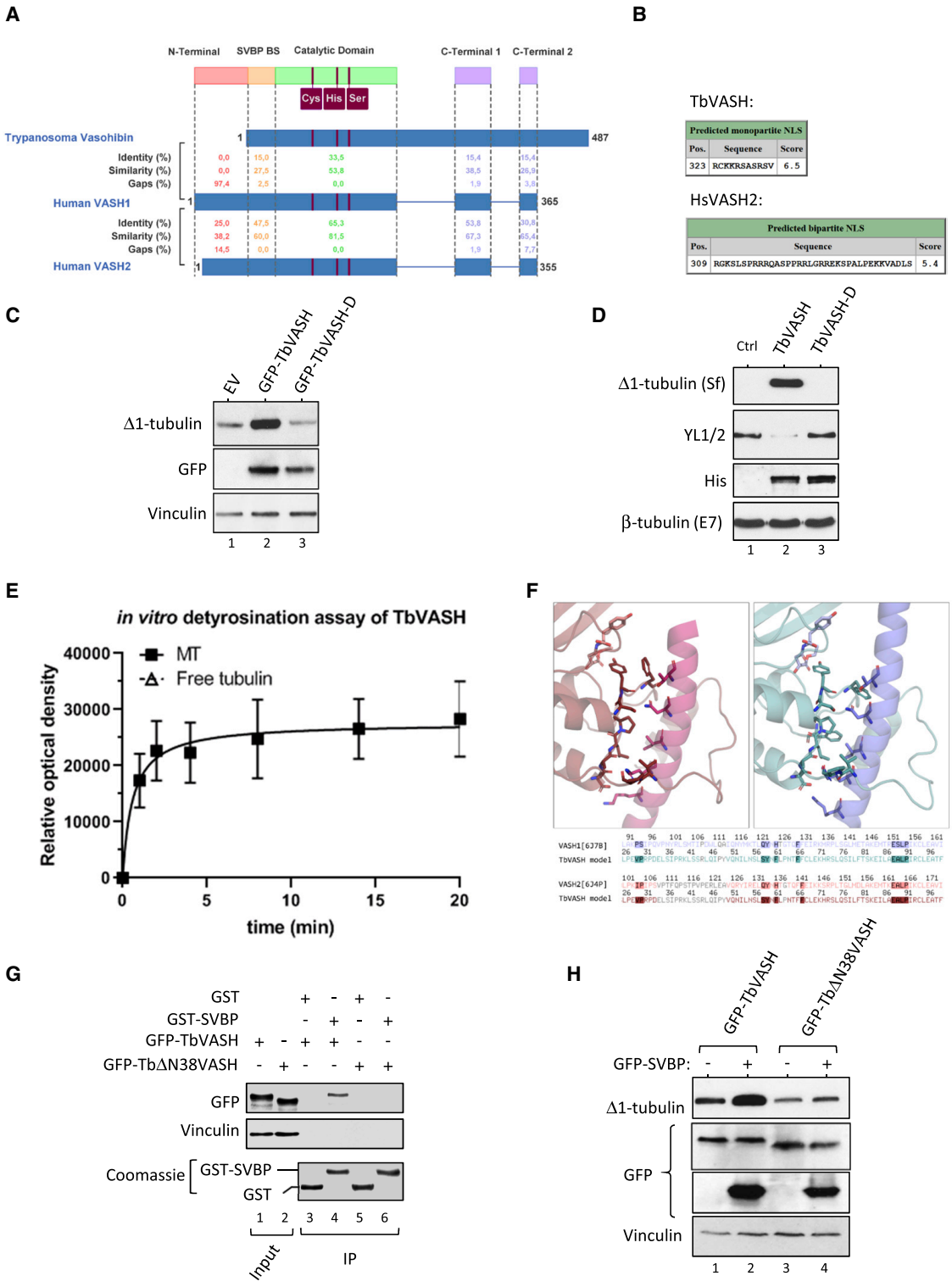

Figure 4. The VASH Gene in *Trypanosoma brucei* (Tb) Possesses Tubulin Detyrosinase Activity

(A) Sequence homology between TbVASH and human VASH1 and VASH2.

(B) Identification of the nuclear localization signal in TbVASH and human VASH1 and VASH2 sequences using an NLS mapper (nls-mapper.iab.keio.ac.jp).

(C) Detyrosinase activity of TbVASH. Ectopic expression of TbVASH and the enzymatically dead (Cys-Ala) protein in HEK293 cells. Twenty-four h after transfection, cells were collected and analyzed by immunoblotting with the indicated antibodies.

(legend continued on next page)

the N-terminal domain contains the SVBP binding site. Deletion of the domain resulted in complete loss of interaction (Figure 4G). Strikingly, co-transfection of full-length TbVASH with SVBP in human HEK293 cells led to an increase in detyrosination activity, whereas Tb-ΔN38-VASH was insensitive to the presence of SVBP (Figure 4H). Thus, the domain required for interaction with SVBP appears to be already present in TbVASH despite the absence of a homologous gene for SVBP, which only appeared more than a billion years later.

Deletion of TbVASH Results in Elongated Parasites with Growth Defects

Using a recently developed CRISPR method (Beneke et al., 2017), we generated procyclic TbVASH-null mutant parasites, as demonstrated by PCR-based analysis (Figures S5A and S5B). To study the consequences of TbVASH deletion at the protein level, we raised *Trypanosoma*-specific antibodies for detyrosinated α- and β-tubulin (Figure 5A). As shown previously by immunofluorescence labeling, we observed that, in wild-type parasites, tyrosinated tubulin (YL1/2 staining) was strong in posterior ends and basal bodies as well as in growing new flagella (Sherwin et al., 1987). In contrast, detyrosination was observed globally over the entire cells, with the exception of the posterior ends (Figure 5B). Strikingly, staining for both detyrosinated α- and β-tubulin was lost in knockout (KO) parasites, suggesting that TbVASH catalyzes the modifications on both tubulin subunits (Figure 5B, bottom panel). Moreover, we observed increased labeling of tyrosinated tubulin, which became evenly distributed throughout the cells (Figure 5B). In agreement, immunoblot analysis of cell lysates further confirmed complete loss of α- and β-tubulin detyrosination in TbVASH KO cells and a simultaneous increase in the level of tyrosinated tubulin (Figure 5C). The activity of TbVASH toward β-tubulin was further validated using purified tubulin from *Trypanosoma* in an *in vitro* detyrosination assay (Figure S5C). In addition, TbVASH KO parasites did not display detectable changes in other tubulin modifications, such as acetylation or polyglutamylation (Figure 5C). Moreover, severe growth defects in KO parasites were observed and confirmed by proliferation assays (Figure 5D). Scanning electron microscopy further revealed abnormally elongated parasites in a Tb-VASH-deficient cell line (Figure 5E), reminiscent of a previously reported nozzle-like morphology (Hendriks et al., 2001). This phenotype was further confirmed by direct measurement of the distance between nuclei and posterior ends to assess parasite length (Figure 5F). Based on the previously described high levels of detyrosination in *Trypanosoma* flagella (Sasse and Gull, 1988), we anticipated functional defects in these structures. However, despite complete loss of detyrosination in KO parasites, the cells did not display major motility defects or striking flagellar abnormalities (Figure S5D). In addition, immunofluorescence analysis demonstrated that attachment of flagella to the cell body was not affected (Figure S5E). Taken together, although no obvious flagellar defects could be observed, we show that, in the absence of detyrosination, parasites displayed profound morphological defects and a strongly reduced proliferation rate.

TbVASH KO Parasites Display Mitotic Defects

To further study the mechanism underlying the growth defects, we analyzed the localization of TbVASH in parasites expressing inducible GFP-TbVASH. Remarkably, we found overexpressed GFP-TbVASH to be mostly localized in the nucleus (Figure 6A), which is consistent with the presence of a predicted NLS in its sequence (Figure 4B). Moreover, in parasites undergoing mitosis, we also detected GFP staining on the spindle, supporting the notion that spindle MTs are directly subjected to TbVASH-mediated detyrosination. This observation was corroborated by YL1/2 labeling of spindle MTs in KO parasites (Figure 6B), which was absent in the wild-type counterparts (Sasse and Gull, 1988). Moreover, spindle MTs were also positively labeled using antibodies specific to detyrosinated β-tubulin (Figure S6A). The bulk DNA content of TbVASH KO parasites revealed a marked broadening of G1 and G2 peaks (Figure S6B), suggesting cell cycle defects. Moreover, TbVASH KO cells displayed an increased forward scatter signal intensity consistent with increased cell size (Figure 6C). To confirm the potential link between morphological defects and cell cycle progression, we counted the number of nuclei and mitochondrial DNA, called kinetoplasts. We observed a decrease in post-mitotic (2 nuclei, 2 kinetoplasts [2N2K]) cells and appearance of anucleated parasites (0N1K), called zoids, in the TbVASH KO cell line (Figure 6D). We further analyzed chromosomal abnormalities using a fluorescence *in situ* hybridization (FISH) probe specifically targeting chromosome 1. TbVASH KO cells revealed a decrease in disomic cells and increased numbers of parasites having a single chromosome 1 (Figure 6E). Taken together, parasites lacking detyrosination displayed increased cell size, defective cell cycle progression, and abnormal chromosomal distribution.

The striking increase in the number of zoids in the absence of TbVASH suggests completion of cell division without chromosome segregation. Given the absence of mitotic checkpoint mechanisms in *Trypanosoma* (Hammarton, 2007), we further aimed to study the consequences of VASH2 depletion in human diploid cycling cells, such as RPE-1 cells. We optimized the experimental conditions for depletion of VASH2 in human cells

(D) *In vitro* detyrosination assay using recombinant TbVASH and the dead mutant (Cys-Ala). The assay was performed on MT polymerized from Sf9-purified tubulin. Reactions were stopped after 30 min and analyzed by immunoblotting with the indicated antibodies.

(E) *In vitro* time course analysis of TbVASH-mediated tubulin detyrosination. Comparison of detyrosination activity on microtubules and free tubulin was performed. Samples were analyzed by immunoblotting, and relative optical density of three independent assays was measured (n = 3; error bars represent SEM). Of note, for free tubulin TbVASH activity was below detection level.

(F) Structural alignment of the SVBP binding sites of hVASH1 (PDB: 6J7B; red) and hVASH2 (PDB: 6J4P; blue) with TbVASH.

(G) GST-SVBP pull-down assays of ectopically expressed TbVASH constructs in HEK293 cells. Pull-down assays were immunoblotted with the indicated antibodies.

(H) Expression of TbVASH N-terminally truncated TbVASH in the absence or presence of SVBP in HEK293 cells. Twenty-four h after transfection, cells were collected and analyzed by immunoblotting with the indicated antibodies.

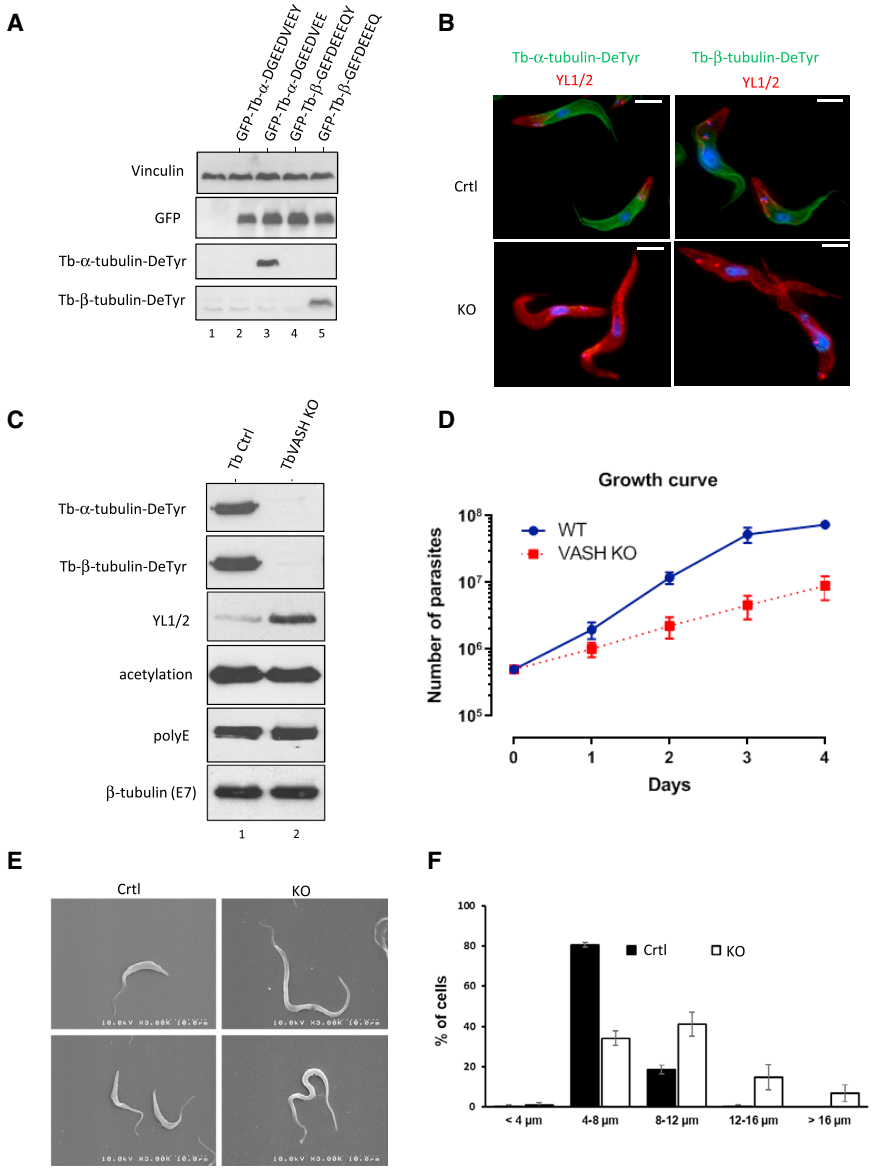

Figure 5. Growth and Cell Cycle Progression Defects of TbVASH Knockout Parasites

(A) Characterization of the *Trypanosoma brucei*-specific detyrosinated tubulin antibodies. Shown is immunoblot analysis of HEK cells transfected with the indicated tubulin constructs. Twenty-four h after transfection, samples were collected and analyzed by immunoblotting with the indicated antibodies.

(B) Immunofluorescence analysis of wild-type (control) and TbVASH knockout (KO) parasites. Cells were stained for detyrosination on both α-tubulin (left panel) and β-tubulin (right panel).

(C) Immunoblot analysis of posttranslational modifications (PTMs) of microtubules in protein extracts obtained from parental and TbVASH KO parasites. Both α- and β-tubulin detyrosination was detected using specific antibodies.

(D) Culture growth curve of parental and TbVASH KO parasites over 4 days (n = 5; error bars represent SD). TbVASH KO parasites display severe growth defects.

(E) Scanning electron microscopy images of representative parental and TbVASH KO parasites. Scale bars, 10 µm.

(F) Cell size analysis of wild-type control and TbVASH KO parasites (n = 3; error bars represent SD).

(Figure S6C) and analyzed the effect of VASH2 knockdown on cell cycle distribution using a bromodeoxyuridine (BrdU) incorporation assay. In the absence of VASH2, we observed a marked increase in the number of BrdU-negative cells having 4n content, pointing to activation of a mitotic checkpoint (Figure S6D). Thus, we monitored the time in mitosis of each individual cell by time-lapse microscopy (Figure S6F). We found that, in the absence of VASH2, cells spent more time in mitosis (Figures S6E and S6F), suggesting that they have difficulties in progressing through mitosis. Finally, to evaluate potential compensatory mechanisms in these cells, we measured, by qPCR, the expression of relevant cell cycle- and cytoskeleton-related genes (Figure S6G). We found that CYC7 and CYC10 were upregulated, likely suggesting that these genes may contribute to the adaptation process (Liu et al., 2013).

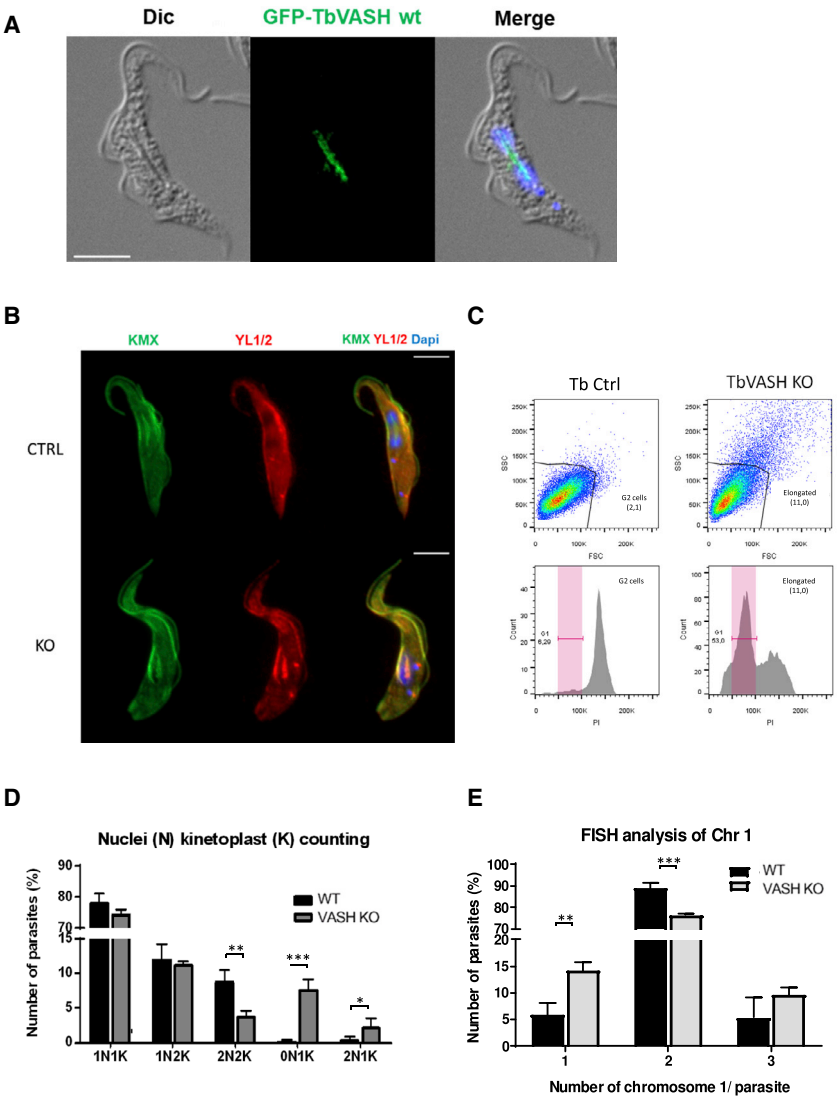

Figure 6. Mitotic Defects in TbVASH Knockout Parasites

(A) Cellular localization of the GFP-TbVASH enzyme in *Trypanosoma brucei*. Scale bar, 5 μm.

(B) Immunofluorescence analysis of control (Ctrl) and TbVASH KO parasites. Cells were stained with the indicated antibodies.

(C) Single-cell analysis of cell size and granularity by flow cytometry. Top panels: side scatter (SSC) versus forward scatter (FSC) density plot analysis of parental and TbVASH knockout parasites. The FSC equates roughly to the size of the cell, and larger cells refract more light than smaller cells. Bottom panels: bulk DNA analysis of cells gated on the large cells only (G2 for parental and "nozzle-like" cells for TbVASH).

(D) Nuclei (N) and kinetoplast (K) counting per cell. An increased number of zoids (0N1K) was observed in the TbVASH KO cell line. (n = 3; error bars represent SD). the p values were calculated using multiple t test analysis (n = 3, * < 0.05, ** < 0.01, *** < 0.001).

(E) Fluorescence *in situ* hybridization (FISH) analysis of wild-type (control) and KO parasites using a chromosome 1-specific probe. Bars indicated mean (n = 3; error bars represent SD). The p values were calculated using multiple t test analysis (n = 3, * < 0.05, ** < 0.01, *** < 0.001).

Using the β-Tubulin Sequence as a Template for Developing TbVASH-Specific Inhibitors

Given the important functions of TbVASH in the life cycle of *Trypanosoma*, inhibition of tubulin detyrosination may provide a meaningful target for treatment of trypanosomatid-related diseases. Because TbVASH catalyzes the removal of the tyrosine not only from α- but also from β-tubulin (Figure 7A), this suggests that the enzymatic pocket differs significantly between human and *Trypanosoma* enzymes. Thus, we aimed to exploit this unique evolutionary feature to design specific peptide-based inhibitors of TbVASH. Given the presence of a highly reactive cysteine residue, VASHs are amenable to covalent inhibition by reactive chemical warheads such as epoxide (Eps). Using an *in vitro* detyrosination assay with recombinant TbVASH, we found that our previously described inhibitor of human VASHs, Eps-Y, also inhibits TbVASH (Figure S7A). By using the C-terminal end of Tb β-tubulin as a scaffold, we developed a series of compounds with higher affinity for TbVASH (Figures 7B and S7B). Surprisingly, changing the COOH group of tyrosine to NH_2 completely abolished the inhibitory effect of the compounds (Figure 7C, compare lanes 3 and 4), likely because of the loss of a stabilizing salt bridge between the inhibitor and the arginine surrounding the active pocket (Adamopoulos et al., 2019; Liao et al., 2019). Moreover, the tripeptide EQY alone or modified with a reactive NO_2 group (compound 3) did not result in any detectable TbVASH inhibition (Figure 7C, compare lanes 3, 5, and 6). Finally, Q-Eps-Y did inhibit Tb-VASH with an estimated the half maximal inhibitory concentration (IC_{50}) around 50 μM (Figure 7D). To assess Q-Eps-Y on human VASHs, we used the human skin melanoma CHL cell line, in which detyrosination mostly depends on hVASH1 and hVASH2 enzymes (Nieuwenhuis et al., 2017). Although Eps-Y inhibited detyrosination at 25 μM, the glutamine-containing compound (compound 4) at the same concentration did not affect the level of detyrosination (Figure 7E). To rule out the possibility that the reduced effect of compound 4 in this system may be due to decreased cell penetration, we overexpressed TbVASH in human HEK293 cells and compared the inhibition of both compounds. As expected, both inhibitors resulted in similar inhibition of TbVASH-dependent detyrosination (Figure 7F). Finally, based on recently published structural data of hVASH1 and hVASH2 bound to Eps-Y in complex with SVBP (Liao et al., 2019), we modeled Tb-VASH using both structures as a template (Figure S7C). Because our data provide evidence that hVASH2 is more closely related to TbVASH, we

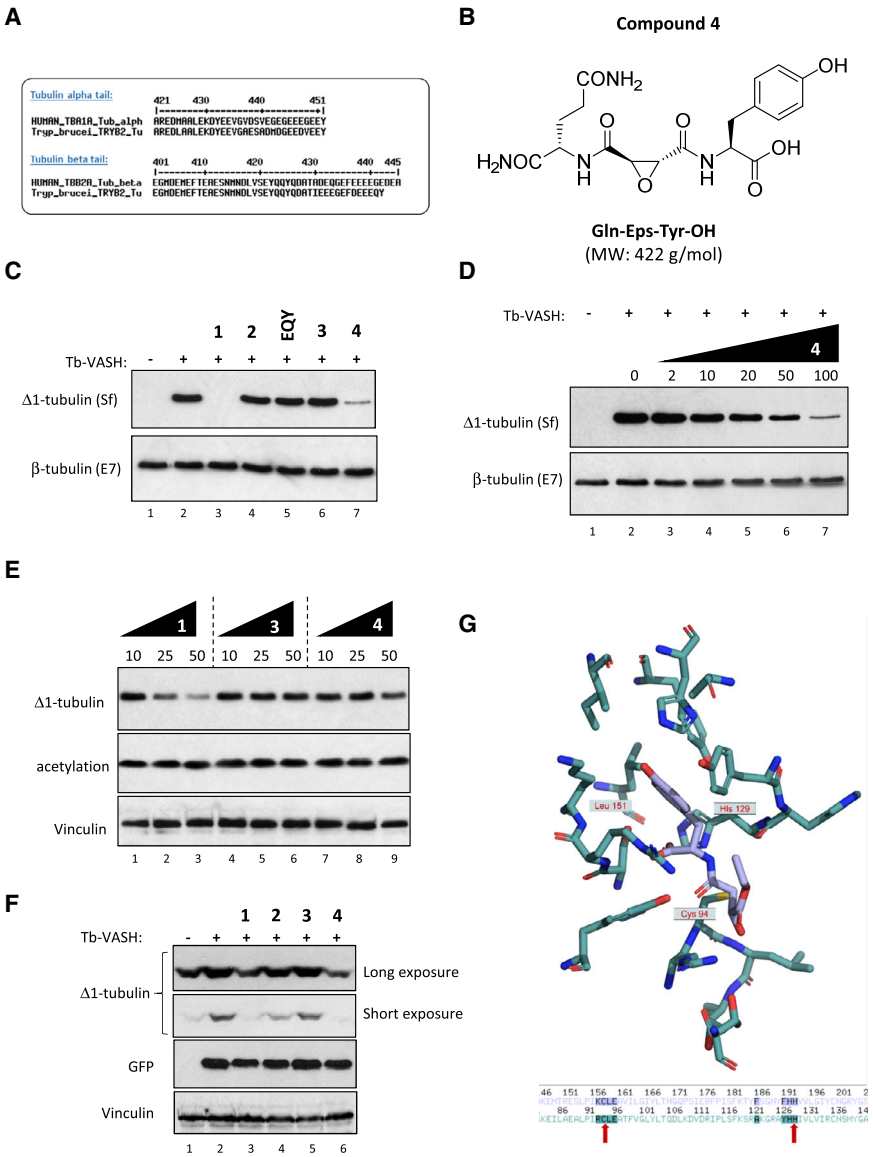

Figure 7. Using Unique Features of *T. brucei* to Develop Peptide-Based Inhibitors of TbVASH

(A) Sequence alignment of the C-terminal tails of both human α Tub1A and TubB2A proteins with corresponding counterparts of *T. brucei* tubulin sequences.

(B) Schematic drawing of Q-Eps-Y (compound 4). The Q-Eps-Y compound was designed based on the C-terminal sequence of *T. brucei* β-tubulin.

(C) *In vitro* detyrosination assay using recombinant TbVASH in the absence or presence of 100 μM compound. The assay was performed in the presence of 0.5 μM microtubules. Reactions were stopped after 15 min and analyzed by immunoblotting with the indicated antibodies.

(D) Dose-response analysis of compound 4 as an inhibitor of TbVASH. Shown is an *in vitro* detyrosination assay using recombinant TbVASH in the presence of increasing concentrations (2–100 μM) of compound 4. The assay was performed in the presence of 0.5 μM microtubules. The reactions were stopped after 15 min and analyzed by immunoblotting with the indicated antibodies.

(E) Dose-response analysis of compounds 1, 3, and 4 *in cellulo*. HEK293 cells were treated with increasing amounts of inhibitors and collected 24 h after treatment. The cells were collected and analyzed by immunoblotting with the indicated antibodies.

(F) Inhibition of ectopically expressed TbVASH in cells. Shown is ectopic expression of TbVASH in HEK293 cells and 24 h treatment with the indicated inhibitor. Following treatment, cells were collected and analyzed by immunoblotting with the indicated antibodies.

(G) Structural model of TbVASH with the catalytic domain bound to compound 1 (Eps-Y). Human VASH2 was used as a template to model TbVASH because both enzymes seem to be functionally more related.

further present the model of the Eps-Y ligand in the catalytic pocket of Tb-VASH based on the structure of VASH2 (Figure 7G). Thus, the unique β-tubulin sequence of TbVASH may be a promising scaffold for rational drug design to limit multiplication of the parasite. Such compounds could be further developed and assessed as innovative drugs to treat trypanosomid-related diseases and should have improved safety profiles because of their selectivity toward parasites enzymes.

DISCUSSION

Here we found that VASH1 requires binding of SVBP tubulin detyrosinating activity, whereas VASH2 has autonomous activity. Moreover, we demonstrate that SVBP acts as *bona fide* activator of both enzymes. Because the presence of two VASH genes in vertebrate species complicates phenotypic analysis, we used *Trypanosoma brucei*, a divergent eukaryote that possesses only a single VASH gene, as a model organism. We show that TbVASH knockout parasites display severe growth abnormalities likely related to mitotic progression defects. Moreover, we present a rational method and the proof of concept for design of inhibitors of TbVASH based on a unique evolutionary feature of β-tubulin in *Trypanosoma* that could potentially serve further drug development.

Vertebrate genomes show evidence of widespread gene duplication (Panopoulou et al., 2003), which might explain the appearance of two independent VASH genes specifically in vertebrates. Typically, in such cases, one copy either degenerates and becomes inactive or undergoes functional specialization, allowing development of more complex regulatory mechanisms (Dehal and Boore, 2005). Because both VASH1 and VASH2 are enzymatically active (Figure S1A), these observations may reflect the increased complexity of the regulatory mechanisms governing α-tubulin detyrosination. Moreover, the appearance

of SVBP in vertebrates may have further contributed to the increased complexity of neuronal organization (Aillaud et al., 2017; Erck et al., 2005; Gundersen and Bulinski, 1986b; Iqbal et al., 2019). In contrast, hVASH2, which acts as an autonomous detyrosinase, seem to be more related to TbVASH and does not depend on the presence of SVBP for activity. In view of the closed mitosis in *Trypanosoma*, the presence of an NLS motif in TbVASH appears to be important for spindle function. Previous study have suggested that the mitotic spindle in *Trypanosoma* is composed exclusively of detyrosinated microtubules. This observation was based on the absence of YL1/2 labeling, which specifically recognizes tyrosinated α-tubulin (Sasse and Gull, 1988). The authors proposed that the spindle is either assembled from already modified tubulin or, alternatively, undergoes rapid post-assembly detyrosination. Our findings that TbVASH does not modify tubulin dimers and that it shows strong localization to the nucleus indicate that spindle detyrosination takes place after MT assembly. Interestingly, despite the absence of a SVBP gene in the *Trypanosoma brucei* genome, we show that a functional binding site is already present in TbVASH and that the interaction leads to increased activity. This suggests that, during evolution, the appearance of the SVBP gene was sufficient to further increase the regulatory complexity of the tubulin detyrosination mechanism, underscoring the functional importance of this modification.

Unexpectedly, TbVASH mutant parasites did not display any visible dysfunction of their flagellum, either in motility or in structure (Figure 5). However, the mutants had abnormally long posterior regions. Increased MT polymerization has been proposed as a potential mechanism for trypanosome cell elongation (Sherwin and Gull, 1989a, 1989b). Because, in the current study, we deleted the enzyme involved in detyrosination, the observed increase in YL1/2 labeling over the entire cell cannot be interpreted as a marker of newly assembled MTs. However, with respect to the thinned shaped of the elongated parasites, we speculate that this results from sliding of MTs past each other, caused by dysregulation of VASH-mediated tubulin detyrosination. This opens the possibility that the differential status of detyrosination regulates motor proteins that cross-link and slide microtubules. These morphological abnormalities might also be a consequence of altered cell cycle progression, as demonstrated previously with mutant parasites displaying a "nozzle-like" morphology (Hammarton et al., 2004; Liu et al., 2013; Tu and Wang, 2004). Furthermore, our data demonstrate that TbVASH mediates detyrosination not only of α- but also of β-tubulin and, therefore, controls the parasite's cell cycle and mitotic division. This makes detyrosination an important signal for parasites to undergo division, likely through pleomorphic functional activities, which include modification of mitotic spindle MTs (Figure 6).

A logical path for developing new therapeutic approaches is to focus on specific features that distinguish the parasites from their human host. Although detyrosination in most species is specific to α-tubulin, both α-and β-tubulins of trypanosomatid parasites are subjected to detyrosination catalyzed by TbVASH (Figure 5). Moreover, the β-tubulin sequence differs significantly from human and *Trypanosoma* α-tubulin sequences, suggesting that the parasite's enzyme has a distinct pocket for catalysis. Because of the presence of a highly reactive cysteine residue in the cleft, this type of protease is amenable to covalent inhibition by reactive chemical warheads such as Eps (Albeck and Kliper, 1997). In *Trypanosoma*, β-tubulin ends with -EQY, in which the negatively charged penultimate glutamate residue is replaced by the non-charged glutamine. Therefore, we generated Q-Eps-Y, which closely resembles the C-terminal sequence of Tb β-tubulin, and show that it preferentially inhibits TbVASH. Further chemical optimization of our compound could provide a potent peptide-based inhibitor of T*rypanosoma* with improved toxicity profiles compared with currently available therapies. Such an approach may be extended to other parasites, such as *Leishmania*, that also possess β-tubulin with a very C-terminal tyrosine residue likely subject to detyrosination.

In summary, we found that SVBP acts as a *bona fide* activator of VASH-mediated tubulin detyrosination, and this is yet another example of the regulatory mechanisms that control the activity of tubulin-modifying enzymes, as we showed recently for glutamylases (Bompard et al., 2018). We show that hVASH2 acts as an autonomous detyrosinase and that, in many respects, it has characteristics similar to TbVASH protein. Although the role of detyrosination in coordinating cell morphogenesis and cell division has already been proposed, our data regarding TbVASH, which modifies cortical and spindle MTs, provides a molecular link between the two processes. Moreover, using an evolutionary unique feature of the Tb β-tubulin C-terminal tail, we provide a method for rational design of small-molecule inhibitors as drugs against trypanosomatid-related diseases.

STAR★METHODS

Detailed methods are provided in the online version of this paper and include the following:

- KEY RESOURCES TABLE
- LEAD CONTACT AND MATERIALS AVAILABILITY
- EXPERIMENTAL MODEL AND SUBJECT DETAILS
  - Cell culture
  - Trypanosoma cell culture and generation of transgenic lines
- METHOD DETAILS
  - Transfection of human cells
  - Multiple alignments and phylogenetic analysis
  - Protein expression and purification
  - *In vitro* characterization of detyrosination activities
  - Flow cytometry
  - Sf insect cells culture and protein production
  - Transmission electron microscopy
  - Fluorescence *in situ* hybridization (FISH)
  - Quantitative PCR
  - Immunofluorescence labeling
  - Mass spectrometry
  - Trypanosoma cell culture and generation of transgenic lines
  - Microscopy
  - Reagents and antibodies
  - Plasmids
- QUANTIFICATION AND STATISTICAL ANALYSIS
- DATA AND CODE AVAILABILITY

SUPPLEMENTAL INFORMATION

Supplemental Information can be found online at https://doi.org/10.1016/j.celrep.2019.11.074.

ACKNOWLEDGMENTS

We would like to thank A. Camasses (IGMM, Montpellier) for reagents; M.P. Blanchard and A. Sarrazin (Montpellier RIO Imaging facility), C. Cazevieille and A. Cabalerro-Megido (MRI-COMET), and M. Lefebvre and L. Crobu (MiVEGEC) for technical assistance; E. Gluenz,S. Dean, and K.Gull (University of Oxford) for generous gifts of plasmids, parasite cell lines, and the anti tubulin antibodies KMX; F. Bringaud (Université Victor Segalen Bordeaux 2) for providing the *T. brucei* cell line and expression vectors; and J. Gaertig (University of Georgia) for critical reading. The work was funded by the French National Research agency ANR under grant numbers: PARAFRAP ANR-11-LABX-0024-01 (to P.B. and Y.S.), EPIGENMED ANR-10-LABX-12-01 (to P.B. and Y.S.), and TYRTUB ANR-13-JSV2-0002 (to K.R.).

AUTHOR CONTRIBUTIONS

Conceptualization, S.v.d.L., M.F.L., and K.R.; Methodology, S.v.d.L., M.F.L., G.M., G.D., Y.L., L.V., and K.R.; Investigation, S.v.d.L., M.F.L., G.M., G.D., L.V., G.B., E.B., Y.L., A.B., S.O., S.U., and K.R.; Supervision, S.v.d.L., M.F.L., and K.R.; Writing – Original Draft, S.v.d.L., M.F.L., and K.R.; Visualization, S.v.d.L., M.F.L., and K.R.; Writing – Review and Editing, Y.S., P.B., M.A., and K.R.; Funding Acquisition, P.B., Y.S., M.A., and K.R.

DECLARATION OF INTERESTS

A patent called "*In vitro* screening assay of tubulin detyrosinase inhibitors" that further describes the use of the assay has been filed (EP 18305958.3).

Received: June 12, 2019
Revised: October 10, 2019
Accepted: November 18, 2019
Published: December 17, 2019

REFERENCES

Adamopoulos, A., Landskron, L., Heidebrecht, T., Tsakou, F., Bleijerveld, O.B., Altelaar, M., Nieuwenhuis, J., Celie, P.H.N., Brummelkamp, T.R., and Perrakis, A. (2019). Crystal structure of the tubulin tyrosine carboxypeptidase complex VASH1-SVBP. Nat. Struct. Mol. Biol. *26*, 567–570.

Aillaud, C., Bosc, C., Peris, L., Bosson, A., Heemeryck, P., Van Dijk, J., Le Friec, J., Boulan, B., Vossier, F., Sanman, L.E., et al. (2017). Vasohibins/SVBP are tubulin carboxypeptidases (TCPs) that regulate neuron differentiation. Science *358*, 1448–1453.

Akera, T., Chmátal, L., Trimm, E., Yang, K., Aonbangkhen, C., Chenoweth, D.M., Janke, C., Schultz, R.M., and Lampson, M.A. (2017). Spindle asymmetry drives non-Mendelian chromosome segregation. Science *358*, 668–672.

Albeck, A., and Kliper, S. (1997). Mechanism of cysteine protease inactivation by peptidyl epoxides. Biochem. J. *322*, 879–884.

Amblard, M., Fehrentz, J.-A., Martinez, J., and Subra, G. (2006). Methods and protocols of modern solid phase Peptide synthesis. Mol. Biotechnol. *33*, 239–254.

Barisic, M., Silva e Sousa, R., Tripathy, S.K., Magiera, M.M., Zaytsev, A.V., Pereira, A.L., Janke, C., Grishchuk, E.L., and Maiato, H. (2015). Mitosis. Microtubule detyrosination guides chromosomes during mitosis. Science *348*, 799–803.

Barra, H.S., Arce, C.A., Rodríguez, J.A., and Caputto, R. (1974). Some common properties of the protein that incorporates tyrosine as a single unit and the microtubule proteins. Biochem. Biophys. Res. Commun. *60*, 1384–1390.

Beneke, T., Madden, R., Makin, L., Valli, J., Sunter, J., and Gluenz, E. (2017). A CRISPR Cas9 high-throughput genome editing toolkit for kinetoplastids. R. Soc. Open Sci. *4*, 170095.

Bessat, M., and Ersfeld, K. (2009). Functional characterization of cohesin SMC3 and separase and their roles in the segregation of large and minichromosomes in Trypanosoma brucei. Mol. Microbiol *71*, 1371–1385.

Bompard, G., van Dijk, J., Cau, J., Lannay, Y., Marcellin, G., Lawera, A., van der Laan, S., and Rogowski, K. (2018). CSAP Acts as a Regulator of TTLL-Mediated Microtubule Glutamylation. Cell Rep *25*, 2866–2877.e5.

Brun, R., and Schonenberger. (1979). Cultivation and in vitro cloning or procyclic culture forms of Trypanosoma brucei in a semi-defined medium. Short communication. Acta Trop *36*, 289–292.

Cambray-Deakin, M.A., and Burgoyne, R.D. (1987). Posttranslational modifications of alpha-tubulin: acetylated and detyrosinated forms in axons of rat cerebellum. J. Cell Biol. *104*, 1569–1574.

Chang, W., Webster, D.R., Salam, A.A., Gruber, D., Prasad, A., Eiserich, J.P., and Bulinski, J.C. (2002). Alteration of the C-terminal amino acid of tubulin specifically inhibits myogenic differentiation. J. Biol. Chem. *277*, 30690–30698.

Ciferri, C., Pasqualato, S., Screpanti, E., Varetti, G., Santaguida, S., Dos Reis, G., Maiolica, A., Polka, J., De Luca, J.G., De Wulf, P., et al. (2008). Implications for kinetochore-microtubule attachment from the structure of an engineered Ndc80 complex. Cell *133*, 427–439.

Dean, S., Sunter, J., Wheeler, R.J., Hodkinson, I., Gluenz, E., and Gull, K. (2015). A toolkit enabling efficient, scalable and reproducible gene tagging in trypanosomatids. Open Biol. *5*, 140197.

Dehal, P., and Boore, J.L. (2005). Two rounds of whole genome duplication in the ancestral vertebrate. PLoS Biol. *3*, e314.

Erck, C., Peris, L., Andrieux, A., Meissirel, C., Gruber, A.D., Vernet, M., Schweitzer, A., Saoudi, Y., Pointu, H., Bosc, C., et al. (2005). A vital role of tubulin-tyrosine-ligase for neuronal organization. Proc. Natl. Acad. Sci. USA *102*, 7853–7858.

Gull, K. (1999). The cytoskeleton of trypanosomatid parasites. Annu. Rev. Microbiol. *53*, 629–655.

Gundersen, G.G., and Bulinski, J.C. (1986a). Distribution of tyrosinated and nontyrosinated alpha-tubulin during mitosis. J. Cell Biol. *102*, 1118–1126.

Gundersen, G.G., and Bulinski, J.C. (1986b). Microtubule arrays in differentiated cells contain elevated levels of a post-translationally modified form of tubulin. Eur. J. Cell Biol. *42*, 288–294.

Gundersen, G.G., Khawaja, S., and Bulinski, J.C. (1989). Generation of a stable, posttranslationally modified microtubule array is an early event in myogenic differentiation. J. Cell Biol. *109*, 2275–2288.

Hammarton, T.C. (2007). Cell cycle regulation in Trypanosoma brucei. Mol. Biochem. Parasitol. *153*, 1–8.

Hammarton, T.C., Engstler, M., and Mottram, J.C. (2004). The Trypanosoma brucei cyclin, CYC2, is required for cell cycle progression through G1 phase and for maintenance of procyclic form cell morphology. J. Biol. Chem. *279*, 24757–24764.

Hendriks, E.F., Robinson, D.R., Hinkins, M., and Matthews, K.R. (2001). A novel CCCH protein which modulates differentiation of Trypanosoma brucei to its procyclic form. EMBO J. *20*, 6700–6711.

Iqbal, Z., Tawamie, H., Ba, W., Reis, A., Halak, B.A., Sticht, H., Uebe, S., Kasri, N.N., Riazuddin, S., van Bokhoven, H., and Abou Jamra, R. (2019). Loss of function of SVBP leads to autosomal recessive intellectual disability, microcephaly, ataxia, and hypotonia. Genet. Med. *21*, 1790–1796.

Kerr, J.P., Robison, P., Shi, G., Bogush, A.I., Kempema, A.M., Hexum, J.K., Becerra, N., Harki, D.A., Martin, S.S., Raiteri, R., et al. (2015). Detyrosinated microtubules modulate mechanotransduction in heart and skeletal muscle. Nat. Commun. *6*, 8526.

Liao, S., Rajendraprasad, G., Wang, N., Eibes, S., Gao, J., Yu, H., Wu, G., Tu, X., Huang, H., Barisic, M., and Xu, C. (2019). Molecular basis of vasohibins-mediated detyrosination and its impact on spindle function and mitosis. Cell Res. *29*, 533–547.

Liu, Y., Hu, H., and Li, Z. (2013). The cooperative roles of PHO80-like cyclins in regulating the G1/S transition and posterior cytoskeletal morphogenesis in Trypanosoma brucei. Mol. Microbiol. *90*, 130–146.

Meyer, A., and Schartl, M. (1999). Gene and genome duplications in vertebrates: the one-to-four (-to-eight in fish) rule and the evolution of novel gene functions. Curr. Opin. Cell Biol. *11*, 699–704.

Mizuno, N., Toba, S., Edamatsu, M., Watai-Nishii, J., Hirokawa, N., Toyoshima, Y.Y., and Kikkawa, M. (2004). Dynein and kinesin share an overlapping microtubule-binding site. EMBO J. *23*, 2459–2467.

Nieuwenhuis, J., Adamopoulos, A., Bleijerveld, O.B., Mazouzi, A., Stickel, E., Celie, P., Altelaar, M., Knipscheer, P., Perrakis, A., Blomen, V.A., and Brummelkamp, T.R. (2017). Vasohibins encode tubulin detyrosinating activity. Science *358*, 1453–1456.

O'Hagan, R., Piasecki, B.P., Silva, M., Phirke, P., Nguyen, K.C., Hall, D.H., Swoboda, P., and Barr, M.M. (2011). The tubulin deglutamylase CCPP-1 regulates the function and stability of sensory cilia in C. elegans. Curr. Biol. *21*, 1685–1694.

Panopoulou, G., Hennig, S., Groth, D., Krause, A., Poustka, A.J., Herwig, R., Vingron, M., and Lehrach, H. (2003). New evidence for genome-wide duplications at the origin of vertebrates using an amphioxus gene set and completed animal genomes. Genome Res. *13* (*6A*), 1056–1066.

Preston, S.F., Deanin, G.G., Hanson, R.K., and Gordon, M.W. (1979). The phylogenetic distribution of tubulin:tyrosine ligase. J. Mol. Evol. *13*, 233–244.

Rogowski, K., van Dijk, J., Magiera, M.M., Bosc, C., Deloulme, J.C., Bosson, A., Peris, L., Gold, N.D., Lacroix, B., Bosch Grau, M., Bec, N., Larroque, C., Desagher, S., Holzer, M., Andrieux, A., Moutin, M.J., and Janke, C. (2010). A family of protein-deglutamylating enzymes associated with neurodegeneration. Cell *143*, 564–578.

Roll-Mecak, A., and Vale, R.D. (2008). Structural basis of microtubule severing by the hereditary spastic paraplegia protein spastin. Nature *451*, 363–367.

Sasse, R., and Gull, K. (1988). Tubulin post-translational modifications and the construction of microtubular organelles in Trypanosoma brucei. J. Cell Sci. *90*, 577–589.

Sato, Y. (2013). The vasohibin family: a novel family for angiogenesis regulation. J. Biochem. *153*, 5–11.

Schneider, A., Plessmann, U., and Weber, K. (1997). Subpellicular and flagellar microtubules of Trypanosoma brucei are extensively glutamylated. J. Cell Sci. *110*, 431–437.

Sherwin, T., and Gull, K. (1989a). Visualization of detyrosination along single microtubules reveals novel mechanisms of assembly during cytoskeletal duplication in trypanosomes. Cell *57*, 211–221.

Sherwin, T., and Gull, K. (1989b). The cell division cycle of Trypanosoma brucei: timing of event markers and cytoskeletal modulations. Philos. Trans. R. Soc. Lond. B Biol. Sci. *323*, 573–588.

Sherwin, T., Schneider, A., Sasse, R., Seebeck, T., and Gull, K. (1987). Distinct localization and cell cycle dependence of COOH terminally tyrosinolated alpha-tubulin in the microtubules of Trypanosoma brucei. J. Cell Biol. *104*, 439–446.

Skiniotis, G., Cochran, J.C., Müller, J., Mandelkow, E., Gilbert, S.P., and Hoenger, A. (2004). Modulation of kinesin binding by the C-termini of tubulin. EMBO J. *23*, 989–999.

Suzuki, Y., Kobayashi, M., Miyashita, H., Ohta, H., Sonoda, H., and Sato, Y. (2010). Isolation of a small vasohibin-binding protein (SVBP) and its role in vasohibin secretion. J. Cell Sci. *123*, 3094–3101.

Trifinopoulos, J., Nguyen, L.T., von Haeseler, A., and Minh, B.Q. (2016). W-IQ-TREE: a fast online phylogenetic tool for maximum likelihood analysis. Nucleic Acids Res *44*, W232–W235.

Tu, X., and Wang, C.C. (2004). The involvement of two cdc2-related kinases (CRKs) in Trypanosoma brucei cell cycle regulation and the distinctive stage-specific phenotypes caused by CRK3 depletion. J. Biol. Chem. *279*, 20519–20528.

Verhey, K.J., and Gaertig, J. (2007). The tubulin code. Cell Cycle *6*, 2152–2160.

Warn, R.M., Harrison, A., Planques, V., Robert-Nicoud, N., and Wehland, J. (1990). Distribution of microtubules containing post-translationally modified alpha-tubulin during Drosophila embryogenesis. Cell Motil. Cytoskeleton *17*, 34–45.

Wehland, J., Willingham, M.C., and Sandoval, I.V. (1983). A rat monoclonal antibody reacting specifically with the tyrosylated form of alpha-tubulin. I. Biochemical characterization, effects on microtubule polymerization in vitro, and microtubule polymerization and organization in vivo. J Cell Biol *97*, 1467–1475.

Westermann, S., and Weber, K. (2003). Post-translational modifications regulate microtubule function. Nat. Rev. Mol. Cell Biol. *4*, 938–947.

Widlund, P.O., Podolski, M., Reber, S., Alper, J., Storch, M., Hyman, A.A., Howard, J., and Drechsel, D.N. (2012). One-step purification of assembly-competent tubulin from diverse eukaryotic sources. Mol. Biol. Cell *23*, 4393–4401.

Winkelhaus, S., and Hauser, M. (1997). Ortho-vanadate affects both the tyrosination/detyrosination state of spindle microtubules and the organization of XTH-2 spindles. Eur. J. Cell Biol. *73*, 306–315.

Wirtz, E., Leal, S., Ochatt, C., and Cross, G.A. (1999). A tightly regulated inducible expression system for conditional gene knock-outs and dominant-negative genetics in Trypanosoma brucei. Mol. Biochem Parasitol *99*, 89–101.

STAR★METHODS

KEY RESOURCES TABLE

REAGENT or RESOURCE	SOURCE	IDENTIFIER
Antibodies		
Δ1-tubulin	Rogowski et al., 2010	N/A
GFP	Torrey Pines Biolabs	TP401
vinculin	Sigma-Aldrich	V9131
hVASH1	Merck-Millipore	MABC537
hVASH2	Merck-Millipore	MABC536
HA	Covance	MMS-101R 16B12
polyHistidine	Sigma-Aldrich	H1029
β-tubulin	Developmental Studies Hybridoma Bank	E7
SVBP/CCDC23	Sigma-Aldrich	HPA008507
YL1/2	John Kilmartin (Wehland et al., 1983)	N/A
acetyl-K40	Sigma-Aldrich	MABT868
polyE	Rogowski et al., 2010	N/A
α-tubulin	Developmental Studies Hybridoma Bank	12G10
PFR2	McMahon-Pratt, Yale	2E10B7
Spodoptera frugiperda Δ1-tubulin	This study	C-GEGEGAEE (peptide)
Bacterial and Virus Strains		
BL21	New England Biolabs	C2530H
DH5α	New England Biolabs	C2987I
baculostrains		N/A
Chemicals, Peptides, and Recombinant Proteins		
Aprotinin	Sigma-Aldrich	10820
Pepstatin	Sigma-Aldrich	P5318
Leupeptin	Sigma-Aldrich	L2884
IPTG	Sigma-Aldrich	V3951
JetPI	Polyplus	101-40N
Interferin	Polyplus	409-50
Carboxypeptidase A	Sigma-Aldrich	C9268
Human hVASH1	This study	N/A
Human hVASH2	This study	N/A
Human SVBP	This study	N/A
Trypanosoma brucei TbVASH	This study	N/A
Experimental Models: Cell Lines		
Human Bone Osteosarcoma Epithelial Cells (U2OS)	Rogowski et al., 2010	N/A
Human embryonic kidney cells 293 (HEK293)	Rogowski et al., 2010	N/A
Sf9 insect cells		N/A
Sf21 insect cells		N/A
Experimental Models: Organisms/Strains		
T. brucei brucei procyclic 29-13	Wirtz et al., 1999	N/A
T. brucei brucei SmOx P9 pTB011	Beneke et al., 2017	N/A
Oligonucleotides		
Hs_vasohibin 1 (Left) CACGTGCTCAAGAAGGTGAA	This paper	N/A
Hs_vasohibin 1 (Right) ACATCCTTCTTCCGGTCCTT	This paper	N/A
Hs_vasohibin 2 (Left) GAGCTGATGGACAAGCCATT	This paper	N/A
Hs_vasohibin 2 (Right) AGTGCTCAGATCAGCCACC	This paper	N/A

(*Continued on next page*)

Continued

REAGENT or RESOURCE	SOURCE	IDENTIFIER
hVASH1 RNAi sequence: GGACCGGAAGAAGGAU GUU(dTdT)	This paper	N/A
hVASH2 RNAi sequence: GGGACAUGAGAAUGAA GAU(dTdT)	This paper	N/A
Complete list of used qPCR primers, see Table S2	This paper	N/A
Recombinant DNA		
pEGP-C1-hVASH2	This paper	N/A
pEGP-C1-hVASH2D (Cys to Ala)	This paper	N/A
pEGP-C1-DN65-hVASH2	This paper	N/A
pEGP-C1-DN104-hVASH2	This paper	N/A
pEGP-C1-hVASH2-DC296	This paper	N/A
pEGP-C1-hVASH1	This paper	N/A
pEGP-C1-hVASH1D (Cys to Ala)	This paper	N/A
pEGP-C1-DN76-hVASH1	This paper	N/A
pEGP-C1-DN115-hVASH1	This paper	N/A
pEGP-C1-TbVASH	This paper	N/A
pEGP-C1-TbVASHD (Cys to Ala)	This paper	N/A
pEGP-C1-DN38-TbVASH	This paper	N/A
pGEX6.1-GST-SVBP	This paper	N/A
pRK5-HA-hVASH1	This paper	N/A
pRK5-HA-hVASH2	This paper	N/A
pRK5-HA-SVBP	This paper	N/A
pCold-hVASH1	This paper	N/A
pCold-hVASH1D (Cys to Ala)	This paper	N/A
pCold-hVASH2	This paper	N/A
pCold-hVASH2D (Cys to Ala)	This paper	N/A
pCold-TbVASH	This paper	N/A
pCold-TbVASHD (Cys to Ala)	This paper	N/A
pET-SVBP(no tag)	This paper	N/A
Software and Algorithms		
Flow cytometry analysis	FlowJo	https://www.flowjo.com/solutions/flowjo
Schematic figure representations	ESPript	http://espript.ibcp.fr
Phylogenetic analysis	IQ-TREE	http://iqtree.cibiv.univie.ac.at
Sequence alignment	Ugene	http://ugene.net/
Other		
Histrap HP	GE Healthcare	29051021
Hitrap desalting	GE Healthcare	29048684
QIAGEN plasmid kit	QIAGEN	12143

LEAD CONTACT AND MATERIALS AVAILABILITY

Further information and requests for resources and reagents should be directed to and will be fulfilled by the Lead Contact, Krzysztof Rogowski (krzysztof.rogowski@igh.cnrs.fr). All unique/stable reagents will be made available on request but we may require a payment and/or a completed Materials Transfer Agreement if there is potential for commercial application.

EXPERIMENTAL MODEL AND SUBJECT DETAILS

Cell culture

Human U20S and HEK293 cells were maintained in Dulbecco's modified eagle medium /F-12 GlutaMAX (GIBCO) supplemented with 10% fetal bovine serum and antibiotics (pen/strep). The cells were cultured at 37°C and 5% CO2.

Trypanosoma cell culture and generation of transgenic lines

Procyclic T. brucei brucei 29-13 (Wirtz et al., 1999) and SmOx P9 pTB011 (Beneke et al., 2017) cell lines were cultured at 27°C in SDM 79 medium (Brun and Schonenberger, 1979) supplemented with 10% decomplemented fetal bovine serum (FBS) and 7 μg/ml hemin. To generate TbVASH null mutants, PCR reactions for sgRNA templates and donor DNAs were used according to the published toolkit for genome editing in kinetoplastids (Beneke et al., 2017). Primers were designed using online tools (LeishGEdit.net and http://grna.ctegd.uga.edu).

METHOD DETAILS

Transfection of human cells

Plasmid and siRNA transfections were performed with JetPEI (Polyplus) and Interferin (Polyplus) respectively, according to manufacturer's guidelines. Cells were collected 48 hours after transfection for immunoblot and immunofluorescence analysis.

Multiple alignments and phylogenetic analysis

Multiple sequence alignments of the VASH and SVBP protein families were performed using Unipro UGENE suite with MUSCLE using default parameters. An alignment of human and *T. brucei* VASH proteins was produced using Clustal Omega with default parameters, 200 rounds of iteration, and followed by quality assessment. In all cases, alignments were manually refined and figures were generated using the ESPript 3.0 server (http://espript.ibcp.fr). Manually refined multiple sequence alignments of protein sequences were used for molecular phylogeny analyses using IQ-TREE (http://iqtree.cibiv.univie.ac.at), using maximum likelihood (Trifinopoulos et al., 2016). Branch support was tested with bootstrap analysis (100 replications), and by two single branch tests, i.e., SH-like approximate likelihood ratio test (10) and a Bayes test.

Protein expression and purification

Human hVASH1 and hVASH2 coding regions were cloned in pCold vector with a polyhistidine tag. The SVBP coding region was also cloned both into pGEX vector for GST-tag protein and into modified pET to produce untagged variant. BL21 bacteria were transformed and induced with IPTG for either overnight at 18°C (pCold vectors) or for 4 hours at 30°C (pGEX or pET vectors). Bacteria were collected and disrupted using a HTU-DIGI-F press (Heinemann). Recombinant proteins were purified using nickel-based affinity chromatography (IMAC) according to the manufacturer's protocol (GE Healthcare).

In vitro characterization of detyrosination activities

Sf9 cells were grown, lysed and used for tubulin purification by affinity chromatography as previously described (Widlund et al., 2012). Microtubules were obtained with taxol and stored at −80°C until further use. *In vitro* analysis of detyrosination activities was perfomed using recombinant hVASH1, hVASH2 and TbVASH proteins. Detyrosination assays were performed in 50mM sodium phosphate buffer in presence of 0.5 μM microtubules obtained from Sf9 tubulin. Reactions were stopped by addition of the denaturating loading buffer followed by 5min incubation at 95°C and loaded on SDS-PAGE for immunoblot analysis.

Flow cytometry

For flow cytometry analysis of parasites, single cells were suspended at a density of 10^6 ml^{-1} in 70% methanol, 30% PBS and were incubated at 4°C overnight. Cells were washed in 10 mL of cold PBS, resuspended in 1 mL of PBS containing 10 μg ml^{-1} propidium iodide and 10 μg ml^{-1} RNase A (Sigma), and incubated at 37°C for 45 min. Bulk DNA analysis by flow cytometry was performed with a Miltenyi MACS quant and analysis performed with FlowJo software.

Sf insect cells culture and protein production

Sf9 and Sf21 cells were grown in EX-CELL® 420 Serum-free medium (14420C, Sigma-Aldrich). Cells were maintained between 1 and 10 million cells/ml in shake flasks, at 28 degrees and 140 rpm agitation. For production of human hVASH1, hVASH2 and SVBP cDNAs were cloned into pFastBac vector MAX efficiency DH10Bac. For infection, 40 million Sf21 cells (in 20 ml) were infected with combinations of P2 encoding hVASH1, hVASH2 and SVBP. Coexpression of hVASH1 and hVASH2 with SVBP was performed by mixing 1:1 with respective P2 supernatants. After 48 hours, infected cells were collected by centrifugation and analyzed by immunoblotting.

Transmission electron microscopy

For ultrastructural analysis, parasites were fixed in 3.5% glutaraldehyde in 100 mM phosphate buffer (pH 7.4) overnight at 4C. The samples were rinsed in phosphate buffer and post-fixed in 1% osmic and 0.8% potassium ferrocyanide for 2 hr in the dark at room temperature (RT). After rinsing in phosphate buffer, samples were dehydrated in a series of ethanol solutions (30%–100%) and embedded in EmBed-812/DER 736. Sections were cut on a Leica-Reichert Ultracut E microtome and counterstained with uranyl acetate and lead citrate. Images were acquired with a Hitachi 7100 transmission electron microscope at MRI-COMET Montpellier (France).

Fluorescence *in situ* hybridization (FISH)

Control and knockout parasites were fixed in 4% paraformaldehyde and dehydrated in serial ethanol baths (50%–100%). The probe targeting α/β-tubulin gene cluster on chromosome 1 (Bessat and Ersfeld, 2009) was labeled with tetramethyl-rhodamine-5-dUTP (Roche®) by using the Nick Translation Mix (Roche®). Slides were then hybridized with a heat-denatured DNA probe under a sealed rubber frame at 94°C for 2 min and then overnight at 37°C. The hybridization solution contained 50% formamide, 10% dextran sulfate, 2X SSPE, 250 mg/ml salmon sperm DNA and 100ng of labeled double strand DNA probe. After hybridization, cells were sequentially washed in 50% formamide-2 X SSC at 37°C for 30 min, 2X SSC at 50°C for 10 min, 2X SSC at 60°C for 10 min, 4X SSC at room temperature. Slides were finally mounted in Vectashield with DAPI. To analyze copy number of chromosome, three independent experiments were performed and ~150 cells were counted in each replicate.

Quantitative PCR

Total RNA was isolated with TRIzol reagent (Invitrogen). Reverse transcription was carried out with random hexanucleotides (Sigma) using PrimeScript RT reagent Kit (Takara). Quantitative PCRs were performed using Lightcycler SYBR Green I Master mix (Roche) on Lightcycler apparatus (Roche). All primers used were intronspanning (primer sequences in Supplemental Information). The relative amount of target cDNA was obtained by normalization using geometric averaging of multiple internal control genes (ACTB, HPRT, HMBS, GAPDH, and SDHA). For mRNA expression analysis of Trypanosoma Brucei all qPCR data were obtained by subtraction of genomic amplification.

Immunofluorescence labeling

Methanol fixed U2OS cells were analyzed using a Zeiss Axioimager Apotome microscope after standard immunofluorescence overnight staining. Parasites were fixed for 20 min with 4% (w/v) paraformaldehyde in PBS and allowed to settle onto teflon slides (Thermo Fisher Scientific) before permeabilization for 10 min with 0.2% Triton X-100 in PBS, and blockage with 2% (v/v) FBS in PBS. Cells were incubated overnight with primary antibodies. Cells were washed three times in PBS and incubated 1h with Alexa Fluor 488-conjugated goat anti-rat, goat anti-mouse and Alexa Fluor 555-conjugated goat anti-rabbit secondary antibodies (Invitrogen) and then washed three times in PBS, stained with DAPI and mounted.

Mass spectrometry

Proteins were separated on SDS-PAGE gels (10% polyacrylamide; Mini-Protean TGX Precast Gels; Bio-Rad) and stained with Page Blue Stain (Fermentas). Gel lanes were cut into several gel pieces and destained by three washes in 50% acetonitrile and 50 mM triethylammonium bicarbonate. Proteins were in-gel digested using trypsin (0.5 μg/band; Gold; Promega).

Peptides were then analyzed online by nano-flow HPLC-nanoelectrospray ionization using a Qexactive Plus mass spectrometer (Thermo Fisher Scientific) coupled to a nano- LC system (U3000-RSLC, Thermo Fisher Scientific). Desalting and preconcentration of samples were performed on-line on a Pepmap® precolumn (0.3 × 10 mm; Dionex). A gradient consisting of 0%–40% B in A for 100 min (A: 0.1% formic acid, 2% acetonitrile in water, and B: 0.1% formic acid in 80% acetonitrile) at 300 nl/min, was used to elute peptides from the capillary reverse-phase column (0.075 × 150 mm, Pepmap®, Dionex). Data were acquired using the Xcalibur software (version 4.0). A cycle of one full-scan mass spectrum (375–1,500 m/z) at a resolution of 70,000 (at 200 m/z), followed by 12 data-dependent MS/MS spectra (at a resolution of 17,500, isolation window 1.2 m/z) was repeated continuously throughout the nanoLC separation. Raw data analysis was performed using the MaxQuant software (version 1.5.5.1) with standard settings. Used database consist of Spodoptera frugiperda entries from Uniprot, G3CKA7 sequence (Uniprot) deleted from 1 to 6 amino acids in Cterm and 250 classical contaminants (MaxQuant contaminant database). Relative abundance of peptide was estimated using Skyline 3.6.0.

Trypanosoma cell culture and generation of transgenic lines

For transfection, log phase cultures were washed and resuspended in 500μL of ZPSM buffer pH 7 (132 mM NaCl, 8 mM KCl, 8 mM Na2HPO4, 1.5 mM KH2PO4, 0.5 mM Mg(CH3COO)2, 90 μM C4H6CaO4) prior to electroporation (exponential protocol, 25μF, 1.5 kV, with a Bio-Rad gene pulser 2 electroporator) in 0.4 cm gap cuvettes with generated DNA constructs. . Amplifications of 5′ and 3′ sgRNA templates were performed with primers ML40-ML42 and ML41-ML42, respectively, and repair DNAs with primers ML43-ML44 using pPOTv7-phleomycin and pPOTv7-hygromycin templates (Dean et al., 2015). A total of four PCR products were purified using Wizard SV Gel and PCR clean up system (Promega) and heat-sterilized before transfection of 35 μg of DNA into 3.107 SmOx P9 pTB011 procyclic cells. After parasites selection with 2.5 μg/ml phleomycin and 50 μg/ml hygromycin, genomic DNA was extracted to monitor the loss of TbVASH locus and integration of the resistance cassettes.

Microscopy

All microscopy was performed on Montpellier RIO imaging platform and images processed using OMERO. Scanning electron microscopy (S4000 Hitachi) of T. brucei parasites was perfomed on freshly prepared parasites. Confocal imaging was performed on a Zeiss LSM780 confocal microscope on paraformaldehyde-fixed T. brucei samples.

Reagents and antibodies

TbVASH inhibitors synthesis

All of the Fluorenylmethyloxycarbonyl (Fmoc) protected amino acids and (1-[Bis(dimethylamino)methylene]-1H-1,2,3-triazolo[4,5-b] pyridinium3-oxid hexafluorophosphate) (HATU) were provided by Iris Biotech GmbH. Piperidine, N,N-Diisopropyléthylamine (DIEA), TFA, Triisopropylsilane (TIS), dichloromethane (DCM), 1,2-Dichloroethane (DCE) and N,N-Dimethylformamide (DMF) N-methylpyrrolidinone (NMP) and ethyl ether (EtOEt) were provided by Sigma Aldrich. AmphiSpheres 40 RAM 0.38 mmol/g 75-150 μm resin was purchased from Agilent Technologies. Solvents used for HPLC and LC/MS were of HPLC grade. All final compounds were purified by reversed-phase 18 HPLC and the purity assessed by analytical reversed-phase HPLC.

SPPS procedure

Peptide synthesis was performed using a standard SPPS protocol (Amblard et al., 2006). Each synthesis was performed using FmocRink amide AmphiSpheres 40 resin (0.3(mmol/g). The Fmoc protected amino acids (4 eq), HATU (4 eq) and DIEA (6 eq) were added to the syringe reactor and the mixture was stirred for 1 hour at room temperature. After each coupling reaction, the peptide-resin was submitted to two 5 min deprotection cycles with DMF/piperidine 80/20 v/v solution.

Compounds purification

All crude compounds were purified by preparative HPLC (Waters 4000 apparatus) on a C18 reversed-phase column (C18 Deltapak column, 100 mm x 40 mm, 15 μm, 100 Å) at a flow rate of 50 mL/min of a H2O + 0.1% TFA and CH3CN + 0.1% TFA mixture in gradient mode with UV detection at 214 nm. Fractions containing the pure product were collected and lyophilized.

LC/MS Analyses

Samples were prepared in an acetonitrile/water (50/50 v/v) mixture containing 0.1% TFA. The LC/MS system consisted of a Waters Alliance 2690 HPLC coupled to a Micromass (Manchester, UK) ZQ spectrometer (electrospray ionization mode, ESI+). All analyses were carried out using a C18 Chromolith Flash 25 × 4.6 mm column. A flow rate of 3 ml/ and a gradient of 0%–100% B over 2.5 min of a H2O + 0.1% HCOOH and CH3CN + 0.1% HCOOH mixture in gradient mode with UV detection at 214 nm. Positive-ion electrospray mass spectra were acquired at a solvent flow rate of 100–200 μl/min. Nitrogen was used for both the nebulizing and drying gas. The data were obtained in a scan mode ranging from 200 to 1700 m/z in 0.1 s intervals; ten scans were summed up to obtain the final spectrum. Retention times are given in minutes. Solvents used for HPLC and LC/MS were of HPLC grade.

Synthesis of HO-Epo-Tyr-OtBu (1'')

948mg (4mmol) of HTyrOtBu were dissolved in 10 mL of DMF followed by 0.5ml of DIEA . In a separate beaker were dissolved 132mg (4mmol) of (±) trans-Epoxysuccinic acid (HO-Epo-OH) in 5ml of DMF followed by 1.5ml of DIEA and 1.520 gr (4mmol) of HATU. The obtained yellowed mixture was added in a drop-wise manner to the HTyrOtBu solution. The reaction mixture (RM) was stirred at room temperature (RT) for 30min until no advancement of the reaction was detected by HPLC. The RM was then poured in the 100ml of EtOEt and washed with a mixture of Brine/1M KHSO4 1/1 v/v solution, then washed two times with 1M KHSO4 solution, dried over MgSO4 and concentrated dry to afford 1g of HO-TEPS-Tyr-OtBu (1'') as slightly yellow powder.

Synthesis of EtO-Epo-Tyr-OtBu (1')

200mg (0.57mmol) of 1'' were dissolved in 10 mL of DMF followed by 92.6mg (0.285mmol) of Cs2CO3 and 50μl (0.285mmol) of EtI. The mixture was stirred overnight at RT and additional 25μM (0.143mmol) of EtI were added. The RM was stirred for additional 2 hours and was then poured in 50 mL of EtOAc. The organic phase was then washed with a mixture of water/brine 50/50 and 2 times with saturated solution of NaHCO3. The organic phase was then washed with brine solution, dried of MgSO4 and concentrated dry to afford 182 mg of the product as white powder. The obtained crude product was used for the next reaction without purification.

Synthesis of EtO-Epo-Tyr-OH (1)

182 mg of Compound 1' (0.48mmol) were dissolved in 20ml of TFA and stirred at RT for 1h. The TFA was then concentrated under reduced pressure and the obtained oil was purified by semi-preparative HPLC with a gradient to afford after lyophilisation 70 mg of 1 as white crystals.

Synthesis of EtO-Epo-Tyr-NH2 (2)

Compound HO-Epo-Tyr-NH2 (2′) was synthetized according to general SPPS procedures. The compound was cleaved from the resin by 2h TFA/DCM 80/20 V/V treatment. The TFA/DCM mixture was then concentrated under reduced pressure and the obtained oil was poured into EtOEt. During this treatment compound 2′ crystalized and was recuperated by centrifugation.

190mg of crude compound 2′ (0.65mmol) were dissolved in 1ml of DMF followed by 316 mg of Cs2CO3 (0.975mmom) and 49.3μl of EtI. The reaction mixture was then stirred at RT overnight. The RM was diluted with 10ml of a 1/1/0.001 V/V/V mixture of ACN/H20/TFA and was purified using preparatory C18 reverse-phase HPLC with a gradient from 0/100/0.001 to 30/70/0.001 ACN/H20/TFA over 30min to obtain of 50mg of EtO-Epo-Tyr-NH2 (2) as white crystals.

Synthesis of Ac-GluGlnTyr(NO2)-OH (3)

Fmoc-Tyr(NO2)-OH was attached to 150mg 2-Chlorotrityl chloride resin (cas42074-68-0) 100-200 mesh charged at 1.6 mmom Cl^-/g resin by dissolving 0.7 eq. of Fmoc-Tyr(NO2)-OH and 2 eq. of DIEA in DMF and mixing in with the resin in a syringe reactor for 2 hours. The resin was then washed 3 times DMF, 3 times DCM and SPPS procedure was performed to obtain intermediate 3′ on the resin. The intermediate amine function was acetylated by a DCM/Ac2O 50/50 v/v treatment and treated with a Pip/DMF 20/80 v/v solution to remove eventual adducts to the unprotected OH function of the nitro-tyrosine. The compound was the cleaved from the resin by a

100ml TFA/DCM 50/50 v/v treatment for 2h. The solution was evaporated and 50 mL of EtOEt were added to the remaining oil. Compound 3 precipitated and was removed by centrifugation and then purified by preparative HPLC to obtain 11 mg as slightly green powder.

Synthesis H2N-Gln-Epo-Tyr-OH (4)

Fmoc-Gln(Trt)-OH was attached to 400 mg of rink amide resin (0.38 mmol/gr) according to SPPS and the Fmoc group was deprotected by DMF/pip 80/20 v/v treatment. Then 105mg of compound 1'' (0.3 mmol) were dissolved in 5ml of DMF followed by 150µl of DIEA and 144mg of HATU. The mixture was stirred at RT for 2 min and was then added to the resin in a dropwise manner and stirred for 4 hours. After standard washing steps the peptide was cleaved from the resin by treatment with TFA/DCM 1/1 v/v solution for 2 hours. The solution was concentrated under reduced pressure. 50 mL of EtOEt were added to the remaining oil and the precipitated crude compound 4 was isolated by centrifugation and then purified by preparative HPLC to afford 9.5mg of the product as white crystals.

Plasmids

All DNA sequences were retrieved from the NCBI (https://www.ncbi.nlm.nih.gov/) and TriTryp databases (https://tritrypdb.org/tritrypdb/). The following sequences were cloned from the human and *Trypanosoma brucei* cDNA and inserted into pCold, EGFP or HA tagged vectors. All DNA constructs were cloned by PCR and inserted in pRK5-HA or pEGFP-C1 for expression in HEK293 and U2OS cells. For bacterial production of recombinant proteins, open reading frames were cloned into pCold vector. Point mutations were introduced into hVASH1 and hVASH2 to generate enzymatically dead versions of the proteins (Cysteine to Alanine) by a PCR-based quick-change method.

QUANTIFICATION AND STATISTICAL ANALYSIS

Where relevant, data is represented as the mean of the indicated number of independent replicates. Statistical differences were assessed with an multiple Student's t test (two tailed). Calculations were performed using Prism 7, version 7.0c (GraphPad). Data are represented as means ± standard errors of the mean (SEM) or standard deviations (SD) otherwise mentioned. n indicated the number of individual experiments. P values are indicated within figure legends and on figures as followed: * < 0.05, ** < 0.01, *** < 0.001. Numbers of counted cells are indicated within figure legends when required.

DATA AND CODE AVAILABILITY

The published article includes all datasets generated or analyzed during this study.